

1  
2  
3  
4  
5  
6  
7  
8  
9  
10  
11  
12  
13  
14  
15  
16  
17  
18  
19  
20  
21  
22  
23  
24  
25  
26  
27  
28  
29  
30  
31  
32  
33  
34  
35  
36

**Identifying analogues for Melimoyu, a long-dormant and data-limited volcano in Chile, through hierarchical clustering**

Burgos, V\*<sup>1,2</sup>, Jenkins, S.F.<sup>1,2</sup>, Bono Troncoso, L.<sup>3</sup>, Perales Moya, C. V.<sup>3</sup>, Bebbington, M.<sup>4</sup>, Newhall, C.<sup>5</sup>, Amigo, A.<sup>3</sup>, Prada Alonso, J.<sup>6</sup>, Taisne., B<sup>1,2</sup>

<sup>1</sup>Earth Observatory of Singapore, Singapore

<sup>2</sup>Asian School of the Environment, Nanyang Technological University, Singapore

<sup>3</sup>Red Nacional de Vigilancia Volcánica. Servicio Nacional de Geología y Minería (SERNAGEOMIN). Santiago, Chile.

<sup>4</sup>School of Agriculture and Environment, Massey University, Palmerston North, New Zealand

<sup>5</sup>Mirisbiris Garden and Nature Center, Philippines

<sup>6</sup>Escuela Politécnica Superior, Universidad Autónoma de Madrid, Madrid, Spain

Burgos, V\*

[burg0001@e.ntu.edu.sg](mailto:burg0001@e.ntu.edu.sg)

**February 15, 2023**

**This manuscript is a non-peer reviewed preprint** submitted to Frontiers in Earth Science and has not yet been accepted for publication. Subsequent versions of this manuscript may have different content. If accepted, the final version of this manuscript will be available via the ‘Peer-reviewed Publication DOI’ link on its EarthArXiv web page. Please feel free to contact us with any comments or feedback about our study.

**Abstract**

Melimoyu is a long-dormant and data-limited volcano in the Southern Volcanic Zone (SVZ) in Chile with only two confirmed Holocene eruptions (VEI 5). Determining the frequency-magnitude relationship for Melimoyu is challenging due to data scarcity. To supplement the eruption records, we identify analogue volcanoes for Melimoyu (i.e., volcanoes that behave similarly and are identified through shared characteristics) using a quantitative and objective approach. Firstly, we compiled a global database containing 181 variables describing the eruptive history, tectonic setting, rock composition, and morphology of 1428 volcanoes. This database was filtered primarily based on data availability into an input dataset comprising 37 numerical variables for 438 subduction zone volcanoes. Then, we applied Agglomerative Nesting, a bottom-up hierarchical clustering algorithm on three datasets derived from the input dataset: i) raw data, ii) output from a Principal Component Analysis,

37 and iii) weighted data tuned to minimise the dispersion in the absolute probability per VEI. Lastly, we  
38 identified the best set of analogues by analysing the dispersion in the absolute probability and applying  
39 a set of criteria deemed important by the local geological service, SERNAGEOMIN, and VB. Our  
40 analysis shows that the raw data generates a low dispersion and the highest number of analogues ( $n=20$ ).  
41 More than half of these analogues are in the SVZ, suggesting that the tectonic setting plays a key role  
42 in the clustering analysis. The  $f$ -M relationship modelled from the analogue's eruption data shows that  
43 if Melimoyu has an eruption, there is a 49% probability (50<sup>th</sup> percentile) of it being  $VEI \geq 4$ . Meanwhile,  
44 the annual absolute probability of a  $VEI \leq 1, 2, 3, 4$ , and  $VEI \geq 5$  eruption at Melimoyu is  $4.82 \times 10^{-4}$ ,  
45  $1.2 \times 10^{-3}$ ,  $1.45 \times 10^{-4}$ ,  $9.77 \times 10^{-4}$ , and  $8.3 \times 10^{-4}$  (50<sup>th</sup> percentile), respectively. Our work shows the  
46 importance of using numerical variables to capture the variability across volcanoes and combining  
47 quantitative approaches with expert knowledge to assess the suitability of potential analogues.  
48 Additionally, this approach allows identifying groups of analogues and can be easily applied to other  
49 cases using numerical variables from the global database. Future work will use the analogues to  
50 populate an event tree and define eruption source parameters for modelling volcanic hazards at  
51 Melimoyu.

52

53 **Keywords:** Analogues, Data-limited, Eruption probability, Frequency-Magnitude relationship, Long-  
54 dormant, Hierarchical clustering, Machine learning, Principal Component Analysis.

55

56 **Abbreviations:** AGglomerative NESTing (AGNES), Cumulative Distribution Function (CDF), Global  
57 Volcanism Program (GVP), frequency-Magnitude ( $f$ -M), Interquartile Range (IQR), Liquiñe-Ofqui  
58 Fault Zone (LOFZ), Magnitude (M), Principal Component (PC), Principal Component Analysis (PCA),  
59 Pyroclastic Density Current (PDC), Relative Completeness Date (RCD), Southern Volcanic Zone  
60 (SVZ), Volcanic Explosivity Index (VEI), Volcanoes of the World (VOTW)

## 61 1. Introduction

62 Volcanoes with limited data on past eruptions are prevalent in global catalogues, such as the Volcanoes  
63 of the World VOTW (GVP, 2013) or LaMEVE database (Crosweller et al., 2012). Melimoyu (Chile),  
64 with just two confirmed Holocene eruptions, both VEI 5 (Geoffroy et al., 2018), is one of these data-  
65 limited volcanoes. We consider Melimoyu a long-dormant volcano (i.e., as defined in Burgos et al.  
66 (2022a): “an active or potentially active volcano without recorded eruptions within the last 100 years”);  
67 the last confirmed eruption took place more than 1800 years ago. According to the Specific Volcanic  
68 Risk Ranking of Active Volcanoes of Chile (SERNAGEOMIN, 2019), Melimoyu is a Volcanic System  
69 Type II (i.e., high-risk volcanic system or volcanic system with recent anomalous activity), ranking 28<sup>th</sup>  
70 out of 92 Chilean active volcanoes. The most recent, and only detected unrest at Melimoyu, took place  
71 in May 2010, when there was an increase in the seismic activity, leading to the Alert Level being raised

72 to Green Level 2 (GVP, 2010) out of the seven alert levels available at that time (i.e., Green 1 and 2;  
73 Yellow 1 and 2; and Red 1, 2, and 3 (Bono, L. and Perales, C. personal communication)).

74 Estimating how often a data-limited volcano like Melimoyu erupts and assessing its volcanic hazards  
75 is challenging since the range of past eruptive styles is not well known (Loughlin et al., 2015). Several  
76 factors can prevent us from having comprehensive eruption records, such as historical events and socio-  
77 cultural factors, the capacity to conduct geological studies, the presence of submarine volcanism,  
78 environmental conditions, and accessibility to the study areas (Burgos et al., 2022b; Mead and Magill,  
79 2014; Siebert et al., 2011). Ideally, we can improve the eruption record by collecting new field data  
80 while the volcano is dormant and there is no imminent threat of reactivation. In Melimoyu, a detailed  
81 fieldwork campaign was carried out by Geoffroy (2017), which focused on characterising the deposits  
82 from the two known Holocene eruptions.

83 Despite these recent efforts, the data available for Melimoyu are still scarce. The main causes are the  
84 high erosion rate in the Patagonian Andes caused by the climatic conditions, especially during glacial  
85 periods, resulting in poorly preserved deposits, and the permanent ice cap covering most of Melimoyu's  
86 edifice (Geoffroy et al., 2018; Herman and Brandon, 2015). In addition, the region of Aysén was  
87 occupied only from the late 19<sup>th</sup> century (Marín, 2014), which could have contributed to the lack of  
88 historical accounts of any potential activity in Melimoyu. Therefore, we must rely on analogue  
89 volcanoes (i.e., volcanoes we expect to behave similarly and which are identified through shared  
90 characteristics) to supplement the eruption record.

91 Analogue volcanoes have been typically defined based on location, tectonic setting, morphology,  
92 magma type, eruption style, or a combination of these factors for i) assessing local and regional volcanic  
93 hazards (e.g., Jenkins et al., 2012b; Lindsay and Robertson, 2018; Mastin et al., 2009; Newhall, 1982;  
94 Newhall and Pallister, 2015; Sandri et al., 2014, 2012; Tennant et al., 2021; Tierz et al., 2020); ii)  
95 estimating frequency-Magnitude ( $f$ - $M$ ) relationship (e.g., Hayes et al., 2022; Jenkins et al., 2012a, 2022;  
96 Rodado et al., 2011; Runge et al., 2014; Sheldrake and Caricchi, 2017; Solow, 2001; Whelley et al.,  
97 2015) s; iii) conducting probabilistic eruption forecasts (e.g., Bebbington, 2014; Bebbington and  
98 Jenkins, 2022; Marzocchi et al., 2004; Sheldrake, 2014), and iv) identifying unrest patterns (e.g.,  
99 Acocella et al., 2015; Newhall et al., 2017).

100 One commonly used approach to identify analogues is classifying volcanoes into categorical classes.  
101 For example, Whelley et al. (2015) proposed five categories of volcanoes that combined the  
102 morphology of the edifice, the state of the activity, and the dimension of the summit crater. One  
103 limitation of using categorical classifications is that numerous volcanoes meet the criteria of a given  
104 category. For example, Whelley et al. (2015) identified 102 volcanoes as well-plugged just in SE Asia.  
105 Hayes et al. (2022) showed that classifying volcanoes into broad categories result in large uncertainty  
106 in the  $f$ - $M$  relationship estimations of SE Asia volcanoes, especially when using global analogues.

107 Similarly, Bebbington and Jenkins (2022) demonstrated that intra-eruption forecasting did not improve  
108 when using data from analogues identified from categorical classes of morphology or composition  
109 instead of the entire dataset once the current activity is accounted for.

110 Several studies have proposed different quantitative approaches to identifying analogue volcanoes in  
111 the last two decades. For example, Hone et al. (2007) carried out a cladistic classification of volcanoes  
112 in Honshu (Japan) by combining multiple characteristics split into states (e.g., the amount of basalt  
113 (compositional type characteristic) is divided into five states that range from none to substantial) and  
114 assigning them individually to each volcano. This approach would be time-consuming to apply at a  
115 global scale (Hone et al., 2007). Sobradelo et al. (2010) classified analogous calderas into three groups  
116 with different geodynamic environments by analysing the caldera area. Tierz et al. (2019) developed  
117 VOLCANS, which combines up to five weighted volcanological criteria to obtain an analogy metric.  
118 VOLCANS is designed to identify analogues for one target volcano at a time since the analogy metric  
119 measures the similarity between a given volcanic system in their database and the target volcano (i.e.,  
120 it does not provide groups of analogue volcanoes). A limitation of VOLCANS is that the weights  
121 assigned to each criterion are selected subjectively by the user. This step can be crucial since the  
122 proposed analogues differ depending on the weighting scheme (Tierz et al., 2019), generating notably  
123 different eruption probability estimates (Tierz et al., 2020). More recently, Wang et al. (2022)  
124 introduced the concept of statistical analogues and proposed using a Weibull renewal process to identify  
125 volcanoes with similar inter-eruption repose times. This new approach was successfully implemented  
126 for forecasting eruptions at Tongariro (New Zealand), a well-studied volcano with 79 confirmed  
127 Holocene eruptions in the VOTW database (GVP, 2013). However, the applicability for data-limited  
128 volcanoes has yet to be tested since it requires several observations (i.e., eruption dates) to estimate the  
129 three model parameters with any degree of precision.

130 In this study, we propose using hierarchical clustering to identify analogues quantitatively and  
131 objectively. Clustering algorithms have been used in volcanology for various applications, such as  
132 detecting patterns in seismic data (e.g., Duque et al. (2020) and Unglert et al. (2016)) or classifying  
133 volcanoes based on morphometric data (e.g., Grosse and Kervyn (2018) and Paguican et al. (2021)).  
134 One of the main challenges when clustering data is that the most used algorithms, such as K-mean,  
135 PAM, or GMM (Xu and Tian, 2015), require the optimal number of clusters to be selected before the  
136 application. To avoid this step, we used AGglomerative NESTing (AGNES), a form of bottom-up  
137 hierarchical clustering that produces a dendrogram without having to pre-define the number of clusters.  
138 This advantage allows us to cut the dendrogram at a height that produces a cluster containing at least  
139 50 potential analogues for Melimoyu. Another important advantage of using AGNES is that the  
140 dendrogram can be used to identify analogues for multiple target volcanoes at the same time, which  
141 could also help us understand why volcanoes are being grouped in each cluster.

142 Our application of hierarchical clustering focuses on identifying analogues for Melimoyu for estimating  
143 the frequency-magnitude relationship. Finding analogues for data-limited volcanoes can be challenging  
144 since we cannot use the eruptive history of other volcanoes to identify analogues, especially if we want  
145 to avoid clustering volcanoes based on the number of available eruptions. For this reason, we rely on  
146 numerical variables that describe the tectonic setting, morphology, and rock composition to find similar  
147 volcanoes with the assumption that these factors control eruption rates and/or reflect the eruptive style  
148 and recent eruptive activity (Acocella, 2014; Acocella and Funicello, 2010; Hughes and Mahood, 2011,  
149 2008a; Sheldrake et al., 2020; Weber and Sheldrake, 2022; Whelley et al., 2015). We compiled 181  
150 variables for 1428 volcanoes from multiple sources and applied AGNES to a selection of 37 numeric  
151 variables describing the rock composition, tectonic setting, and morphology of 438 subduction zone  
152 volcanoes (see Section 3.2).

153 The analysis consisted of three steps. First, a sensitivity analysis was performed using three different  
154 datasets to assess how the input data influences the definition of analogues and the performance of the  
155 clustering. Then, we compared the dispersion in the absolute eruption probability (i.e., the annual  
156 probability of an eruption of a given VEI) from the three sets of potential analogues. Next, the  
157 suitability of the analogue volcanoes was assessed by applying specific criteria considered important  
158 by SERNAGEOMIN and VB for being an analogue of Melimoyu (see Section 4.3), such as having a  
159 history of large explosive eruptions ( $VEI \geq 4$ ) in the Holocene. Lastly, the eruption records from the  
160 analogues were used to model the  $f$ -M relationship given by the absolute and conditional (i.e., relative  
161 probability of an eruption of a given VEI, conditional on an eruption has already taken place)  
162 probability.

163 This approach allows us to objectively group volcanoes based on similar volcanic characteristics, assess  
164 the goodness of the clustering using quantitative metrics while accounting for expert knowledge, and  
165 quantify the uncertainty in our analogue-derived estimates of eruption probabilities. Furthermore, we  
166 provide the global database (accessible in supplementary material 1) with 181 variables and 1428  
167 volcanoes so that our approach can be easily applied to other volcanoes or a different selection of  
168 variables.

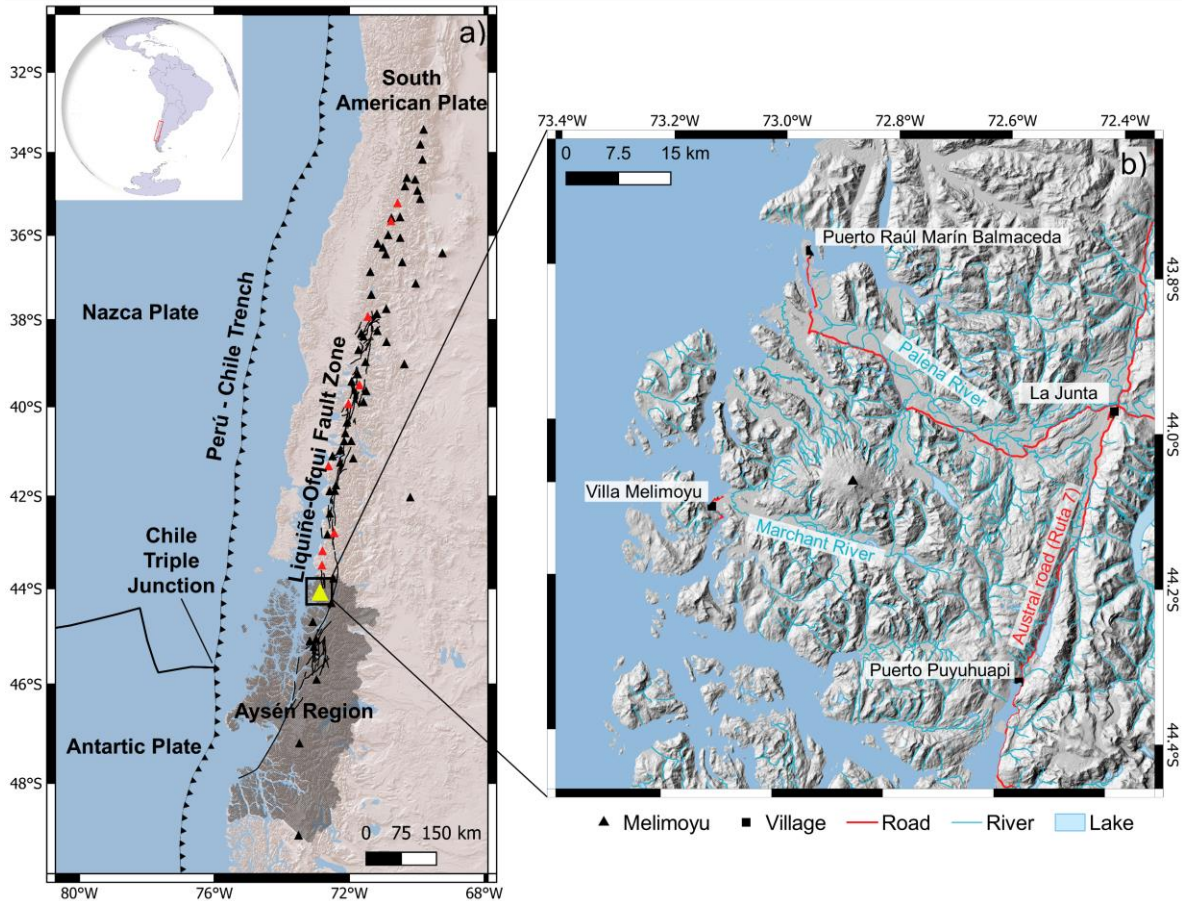
169 In summary, this paper aims to:

- 170 1. Automatically identify analogue volcanoes quantitatively and objectively for Melimoyu.
- 171 2. Assess the influence of the input data on the clustering results through a sensitivity analysis.
- 172 3. Combine quantitative metrics and expert judgement to assess analogue suitability.
- 173 4. Estimate the  $f$ -M relationship for Melimoyu using eruption records from a selection of  
174 analogues.

175 SERNAGEOMIN will use the set of analogues and the f-M relationship to inform the volcanic hazard  
176 matrix and official hazard map for Melimoyu. Future work will explore the application of Melimoyu's  
177 analogues for populating an event tree and identifying eruption source parameters for a probabilistic  
178 long-term hazard assessment. The clustering results are also provided to SERNAGEOMIN so that the  
179 suitability of different potential analogues can be assessed for other data-limited volcanoes in Chile.

## 180 **2. Geological setting**

181 Melimoyu is a 2408 m high ice-capped composite volcano with a 1-km wide crater summit and several  
182 parasitic cinder cones (GVP, 2013). The characteristic oblique subduction in the Chile Triple Junction,  
183 crustal thickness, and Liquiñe-Ofqui Fault Zone (LOFZ) (Fig. 1a) are responsible for the variable nature  
184 of the volcanism, volcanic forms, and rock composition in this area (Cembrano and Lara, 2009; de  
185 Pascale et al., 2021; Völker et al., 2011). The LOFZ intra-arc fault system also controls the spatial  
186 distribution and the type of volcanism of the southern segment of the Southern Volcanic Zone (SVZ),  
187 from Villarrica in the north to Hudson in the south, with contrasting eruptive styles between volcanoes  
188 on the compressive side with wide ranges of compositions and volcanoes on the extensive side with  
189 more primitive magmas (Cembrano and Lara, 2009; de Pascale et al., 2021; Gutiérrez et al., 2005;  
190 López Escobar et al., 1995; Stern et al., 2007). The paleo-seismic Holocene record in the Aysén region  
191 shows that the triggering of several Holocene volcanic eruptions could be closely linked to earthquakes  
192 from the LOFZ and megathrust earthquakes (Watt et al., 2009; Wils et al., 2018).



193

194 **Fig. 1.** Map of the Southern Volcanic Zone (SVZ) (33°S-46°S) a) and surroundings of Melimoyu b).  
 195 Holocene volcanoes from the VOTW database are marked with black triangles, Melimoyu is marked  
 196 with a yellow triangle in a) and with a black triangle in b), analogues of Melimoyu in the SVZ are  
 197 marked with a red triangle. Aysen region is highlighted in dark grey. Plate boundaries extracted from  
 198 Bird (2003), and active and potentially active faults from the Liqueñe-Ofqui Fault Zone (LOFZ)  
 199 extracted from Melnick et al. (2020) are represented with black lines. Basemap a) ESRI Shaded Relief,  
 200 b) ALOS PALSAR DEM 12.5 m resolution.

201 The nearest towns of La Junta (1431 inhabitants; Instituto Nacional de Estadísticas (2019)) and Puerto  
 202 Raúl Marín Balmaceda (239 inhabitants; Instituto Nacional de Estadísticas (2019)) are located around  
 203 40 km to the east and 33 km to the northwest from the volcano (Fig. 1b), respectively, in the sparsely  
 204 populated region of Aysén (e.g., total population of 103,158 according to the last census from 2017  
 205 (Instituto Nacional de Estadísticas, 2019)). Tephra fall deposits are found around these localities,  
 206 suggesting that future eruptions could affect the population in this area and disrupt the Carretera Austral  
 207 (Naranjo and Stern, 2004), which is the only road access to Aysén region (Rojas Hoppe and Subiabre,  
 208 1998). The little village of Villa Melimoyu, with around 100 inhabitants (Instituto Nacional de  
 209 Estadísticas, 2019), located at Marchant River valley around 19 km southwest of the volcano, could

210 also be affected by PDCs or lahars, given the explosive nature of Melimoyu (Geoffroy et al., 2018;  
211 Naranjo and Stern, 2004) and the size of the glaciers in the volcanic edifice (Daros Idalino et al., 2020).

212 The Holocene record from Melimoyu contains two confirmed eruptions: i) Mm-1 dated around 2.8ka  
213 BP, and ii) Mm-2 dated around 1.6ka BP (Geoffroy et al., 2018; Naranjo and Stern, 2004). Geoffroy et  
214 al. (2018) reported that the column height for Mm-1 and Mm-2 ranged between ~30-35 km and ~26-30  
215 km, respectively, establishing that both eruptions had a VEI 5. In addition, several tephra layers found  
216 in lakes and rivers in the area, which dated ~4.6-4.8 ka BP, ~8.3 ka BP, and before the Last Glacial  
217 Maximum at >19,670 BP, have been attributed to Melimoyu due to similarities in the geochemistry,  
218 although their origin and size have not been confirmed (Stern et al., 2015; Weller et al., 2017).

### 219 **3. Data**

#### 220 *3.1 Global database*

221 The global database (supplementary material 1) includes 1428 volcanoes categorised as Holocene in  
222 the VOTW database (v. 4.8.5; 11 February 2020) (GVP, 2013). We excluded 31 volcanoes from the  
223 analysis because they were discontinued from the GVP Holocene Volcano List as of August 2021. Our  
224 database contains 181 variables describing general information from each volcano and its Holocene  
225 eruption record, rock composition, tectonic setting, and morphology.

#### 226 **General information (53 variables)**

227 General information about each volcano and its Holocene eruptive history was obtained from the  
228 VOTW database (GVP, 2013). We included categorical variables describing the tectonic setting,  
229 morphology, and rock composition, the volcano location, date of the most recent eruption, range of VEI  
230 in the Holocene, number of eruptions as a function of VEI, and number of hazards and processes (i.e.,  
231 events in GVP terminology).

#### 232 **Rock composition (17 variables)**

233 The composition was compiled from the VOTW database (GVP, 2013) and the EarthChem Portal  
234 (<http://www.earthchem.org>, downloaded on 31 October 2022, using the parameters: Volcano Name =  
235 All volcanoes, Age = Holocene (0 Ma – 0.01 Ma), Material= Whole rock/rock, and normalization=  
236 Major Elements as Reported). The GVP lists a maximum of five rock types for each volcano, which  
237 were extracted by scraping the profiles from their website. Siebert et al. (2015) classified the  
238 composition into ten rock types: Andesite/Basaltic Andesite, Basalt/Picro-Basalt, Dacite, Foidite,  
239 Phono-tephrite/Tephri-phonolite, Phonolite, Rhyolite, Trachyandesite/Basaltic Trachyandesite,  
240 Trachybasalt/Tephrite Basanite, and Trachyte/Trachydacite.



241 Since the rock types in the GVP are listed in descending order of abundance (Siebert et al., 2015), we  
242 assumed that rock type 1 is five times more abundant than rock type 5 and assigned a weight ranging  
243 from five to one to each of the up to five rock types. We normalised the weights considering the number  
244 of rock types available per volcano and assigned them to each rock type. For example, West Eifel  
245 Volcanic Field (Germany) has the following rock types listed in order of descending abundance:  
246 Foidite, Trachybasalt/Tephrite Basanite, and Phonolite. Since there are three out of five possible rock  
247 types, we add 5, 4, and 3 to a total weight of 12. Then, we assigned 5/12 to Foidite, 4/12 to  
248 Trachybasalt/Tephrite Basanite, 3/12 to Phonolite, and zero to the remaining rock types not listed in the  
249 West Eifel Volcanic Field GVP profile. With this approach, we captured the range of compositions and  
250 the relative abundance.

251 From the dataset downloaded from EarthChem Portal, we filtered the igneous and volcanic samples and  
252 extracted the SiO<sub>2</sub> wt%, from which we calculated the minimum, maximum, median, mean, mode,  
253 standard deviation, and variance across all the available samples per volcano. One limitation we found  
254 when downloading data from multiple volcanoes from the EarthChem portal is that the volcano name  
255 is not associated with the sample name. Therefore, we used the linear distance matrix tool from QGIS  
256 (N\*K\*3) to assign each sample to the nearest volcano. As a result, we have 2090 samples distributed  
257 across 125 volcanoes. The number of samples per volcano ranges from 1 for each of 34 volcanoes to  
258 281 for Vesuvius.

#### 259 **Tectonic setting (44 variables)**

260 One of the variables compiled for the tectonic setting is the total crustal thickness (excluding the water  
261 layer) extracted from the Global Model of Earth's Crust CRUST1 (Laske et al., 2013). We used the  
262 distance matrix tool in QGIS to identify the nearest data point (pair of coordinates set at 1 degree) from  
263 each volcano.

264 We also calculated the distance to the closest plate boundary classes (i.e., oceanic spreading ridge  
265 (OSR), oceanic transform fault (OTF), oceanic convergent boundary (OCB), continental rift boundary  
266 (CRB), continental transform fault (CTF), continental convergent boundary (CCB), and subduction  
267 zone (SUB)) from each volcano (Bird, 2003). We used the midpoints of each digitisation step (end point  
268 of PB2002.dat in Bird (2003)) as the reference point to calculate the distance. We also extracted the  
269 plate boundary identifier and the plate boundary class for the closest boundary class.

270 For volcanoes in subduction zones, we extracted 17 variables from Heuret (2006) describing the relative  
271 and absolute movement of plates at the nearest subduction arc segment (e.g., normal component of the  
272 subducting velocity), the age of the slab and the thermal parameter. The study by Heuret (2006) only  
273 includes non-perturbed subduction zones, which are those distant from a collision zone, ridge, or plateau

274 subduction. Additionally, we used the same arc segment names from Heuret (2006) to extract the  
275 variables slab length, slab pull force, Upper Plate Strain (UPS), and Upper Plate Nature (UPN) from  
276 Lallemand et al. (2005).

277 Lastly, we extracted the depth, dip, strike, and thickness of the slab at each subduction zone volcano  
278 from the Slab2 model developed by Hayes et al. (2018), which is available in the USGS ScienceBase  
279 catalogue (Hayes, 2018).

## 280 **Morphology (64 variables)**

281 To describe the morphology, we used the database from Grosse et al. (2014) and Grosse and Kervyn  
282 (2018), which characterises the morphometry of composite, calderas, and shield volcanoes. The  
283 variables included in these databases describe the edifice size, profile shape, plan shape, and slope  
284 (Grosse et al., 2014). We updated the values in Grosse et al. (2014) with those from Grosse and Kervyn  
285 (2018) for volcanoes included in both studies. Seventeen of the 64 variables compiled from these studies  
286 are only available for calderas or composite volcanoes with large summit craters.

### 287 *3.2 Input dataset*

288 The input dataset for the clustering contains only volcanoes with data for all the selected variables since  
289 we do not allow missing values in the clustering. In addition, we only considered numerical variables  
290 in the analysis, excluding 16 categorical variables, three textual variables, and 13 identifiers. We also  
291 excluded ten uninformative variables, such as the number of elevation contours in Grosse et al. (2014).  
292 As discussed in the introduction, we want to avoid clustering volcanoes based on their degree of  
293 completeness, which, in the case of Melimoyu, would presumably produce analogues that are also data-  
294 limited volcanoes. Therefore, we excluded 36 variables related to eruptive history or style. We also  
295 excluded coordinates since we want to avoid grouping volcanoes by their proximity ( $n=4$ ). Lastly, since  
296 our application of AGNES is targeted at Melimoyu, we excluded 31 variables with missing data for  
297 Melimoyu, among which we have the eight variables calculated from the data extracted from  
298 EarthChem.

299 The remaining variables are considered of interest for our case study. Since we do not allow missing  
300 data in the clustering and most tectonic setting variables describe characteristics of subduction zones,  
301 we automatically exclude volcanoes from other tectonic settings. Therefore, we only retain the distance  
302 to the nearest plate boundary (i.e., subduction zone) and exclude the other seven variables that measure  
303 the distance to different plate boundary types. Lastly, for variables accounting for duplicated  
304 information (e.g., edifice height, basal width, and height/basal width ratio from Grosse et al. (2014)),

305 we preferentially selected variables not calculated as a function of other variables in the database,  
306 leading us to exclude 22 variables.

307 As a result of this filtering, we have 38 numerical variables (10 for rock composition, 14 for tectonic  
308 setting, and 14 for morphology) available for 438 subduction zone volcanoes. Note that Foidite is not  
309 included in the clustering because none of these volcanoes has records of this rock type in the VOTW  
310 database. The input dataset for Melimoyu can be accessed in supplementary material 2, and the  
311 complete list of 37 variables after excluding Foidite is listed in Table 1 and Figure 3.

## 312 **4. Methodology**

### 313 *4.1 Hierarchical clustering*

314 In this study, we used AGNES, a bottom-up hierarchical clustering approach (Kaufman and Rousseeuw,  
315 1991). The main advantage of hierarchical clustering is that it does not require the number of clusters  
316 to be pre-defined. We selected agglomerative instead of divisive hierarchical clustering because the  
317 former tends to identify smaller clusters (Boehmke and Greenwell, 2019). Before applying AGNES,  
318 we calculated the (dis)similarity matrix, which contains the distance among pairs of volcanoes. We  
319 selected the Manhattan distance metric because it performs better than the Euclidean distance for high-  
320 dimensional datasets (Aggarwal et al., 2001), and is less sensitive to outliers (Strauss and Von Maltitz,  
321 2017).

322 In AGNES, each observation (volcano) starts as a single cluster (leaf). Then, based on the Manhattan  
323 distance, the most similar pair of volcanoes are grouped into a bigger cluster (node or branch). Lastly,  
324 the most similar clusters are merged iteratively until all the volcanoes are grouped into one big cluster  
325 (root). The (dis)similarity between clusters is determined by the linkage method. Some commonly used  
326 methods are average linkage, single linkage, complete linkage, and Ward's linkage (we refer the reader  
327 to Kaufman and Rousseeuw (1991) for more details on each method). To select the best linkage method,  
328 we ran AGNES using these four methods and retained the results that produced the highest  
329 agglomerative coefficient – Ward's linkage. The agglomerative coefficient describes the strength of the  
330 clustering structure, with values closer to 1 indicating a strong clustering structure (Kaufman and  
331 Rousseeuw, 1991).

332 The agglomerative coefficient can be considered a form of internal validation of the clustering since it  
333 measures the quality of the clustering structure without reference to external information (Boehmke and  
334 Greenwell, 2019). Another form of internal validation is assessing the clustering tendency of the input  
335 data (Banerjee and Davé, 2004). The clustering tendency evaluates if the dataset contains an inherent  
336 grouping structure. One metric used to assess the clustering tendency is the Hopkins statistic (H), which  
337 estimates the probability that the dataset is generated by a random uniform distribution (Lawson and

338 Jurs, 1990). The input data are highly clusterable when H is close to 1. We used the agglomerative  
339 coefficient and Hopkins statistic metrics to compare the quality of the clustering results from the  
340 sensitivity analysis.

341 The output of AGNES is a dendrogram, a tree-based representation containing leaves, nodes, and the  
342 root. The height of the dendrogram (horizontal axis in Figures 2, 5, and 6) represents the distance (i.e.,  
343 (dis)similarity) between clusters. Note that the height values are not comparable between the  
344 dendrograms presented in this study because they are constructed using different input data. Therefore,  
345 the height can only be used to interpret the similarity between clusters within their dendrogram. The  
346 height at which we cut the dendrogram controls the number of clusters generated. Instead of searching  
347 for the optimal number of clusters, which is the main challenge when using other clustering algorithms,  
348 we found the height that generates a cluster of at least 50 potential analogues for Melimoyu. In this  
349 study, we want to avoid retaining larger numbers of potential analogues so the suitability assessment of  
350 individual volcanoes is not excessively time-consuming. Thanks to the flexibility of AGNES, future  
351 applications can adjust the number of analogues to fit their goal.

352 To compare the similarity between Melimoyu and the potential analogues, we normalised the  
353 Manhattan distance ( $M_{norm}$ ) via min-max normalisation as follows:

$$354 \quad M_{norm} = 1 - \frac{M - M_{min}}{M_{max} - M_{min}} \quad (1),$$

355 where the maximum,  $M_{max}$ , and minimum value,  $M_{min}$ , corresponds to the highest and lowest Manhattan  
356 distance, respectively, within the set of potential analogues, including Melimoyu (i.e.,  $M_{norm}$  ranges from  
357 0 for the least similar volcano to 1 for Melimoyu).

#### 358 *4.2 Sensitivity analysis*

359 We performed a sensitivity analysis on three different input datasets to assess how they change the  
360 outcome of the clustering, which are the proposed analogue volcanoes, and the quality of the results in  
361 terms of internal validation metrics.

##### 362 **Raw dataset**

363 The first application of AGNES was made on the selection of 37 variables. Each variable was  
364 standardised (i.e., centred and scaled) so that the distribution of the transformed data, known as z-score,  
365 had a mean of 0 and a standard deviation of 1 (Han et al., 2012). Standardising the data is an essential  
366 pre-processing step when using machine learning models on data measured with different units,  
367 covering wide ranges of values, or in the presence of outliers since it has been shown to improve the  
368 quality of the clustering (Mohamad and Usman, 2013).

369

370 **Reduced dataset**

371 The preparation of the second input dataset consisted of two steps aimed at capturing the most important  
372 variables by excluding redundant variables and reducing noise in the data.

373 Firstly, we removed five redundant variables from the original dataset of 37 variables and standardised  
374 the dataset. The redundant variables were identified from the correlation between variables. As almost  
375 all the variables are non-normally distributed, we used Kendall's Tau correlation coefficient (Chen and  
376 Popovich, 2002). Lastly, we classified the strength of the correlation as very weak ( $0 < r < 0.2$ ), weak  
377 ( $0.2 \leq r < 0.4$ ), moderate ( $0.4 \leq r < 0.6$ ), strong ( $0.6 \leq r < 0.8$ ), and very strong ( $0.8 \leq r < 1$ ). We used  $r \geq 0.8$  as the  
378 threshold to identify which redundant variables should be excluded from the Principal Component  
379 Analysis (PCA) so that there are no pairs of very strongly correlated variables in the input data. We  
380 remove the variable with the largest mean absolute correlation for very strongly correlated variables.  
381 Although PCA can handle redundant variables, we preferred to include this step to ensure that all  
382 detrimental redundancies were removed from the dataset.

383 Secondly, we applied a PCA to the dataset derived from the first. This approach is used to deal with the  
384 'curse of dimensionality' before using clustering algorithms (Assent, 2012) by transforming the original  
385 variables into uncorrelated Principal Components (PC) through linear combination (Abdi and Williams,  
386 2010). The PCA helps to improve the interpretability of high-dimensional datasets by reducing the  
387 dimensions and capturing the maximum possible variance of the original data. The number of PCs to  
388 retain for the analysis is often based on an arbitrary percentage of the cumulative variance. In this study,  
389 we used a threshold of 70% since it is a commonly used value (Jolliffe and Cadima, 2016), although  
390 other thresholds could be tested to assess the influence of the variance of the input data on the clustering.  
391 The coordinates or scores from each volcano in the retained PCs were used as input data for the  
392 clustering.

393 **Weighted dataset**

394 For the third dataset, we applied a weighting scheme on the raw dataset (i.e., 37 standardised variables)  
395 tuned to minimise the dispersion of the absolute probability from the set of potential analogues. With  
396 this approach, we acknowledge that each variable is unlikely to have equal influence on the clustering  
397 of volcanoes with analogous eruptive behaviour (i.e., similar  $f$ -M relationship).

398 The steps we followed were:

- 399 1. Draw a set of 37 weights from a uniform distribution and normalise so all weights add to one.
- 400 2. Apply AGNES using the best linkage method identified from the raw and reduced dataset  
401 (Ward's linkage) with variables weights from step 1.
- 402 3. Extract a set of at least 50 potential analogues.

- 403 4. Estimate the absolute probability per VEI (i.e., the annual probability of an eruption of a given  
 404 VEI) ( $P_{ABS}$ ) for each analogue volcano  $i$ :

405 
$$P_{ABS\ ij} = \frac{n_{ij}}{t_{ij}} \quad (2),$$

406 where  $n_{ij}$  is the number of recorded eruptions of a given VEI  $j$  (VEI  $\leq 1$ , VEI 2, VEI 3, VEI 4,  
 407 and VEI  $\geq 5$ ) and  $t_{ij}$  is the number of years between the Relative Completeness Date (RCD) and  
 408 2019. We calculate the regional RCDs (i.e., the most complete portion of the catalogue) from  
 409 the VOTW database (GVP, 2013) as a function of each VEI  $j$  using the most abrupt change  
 410 point method from Burgos et al. (2022b) and the 31 new regions proposed in their study  
 411 (supplementary material 3).

- 412 5. Calculate the Interquartile Range ( $IQR_j$ ) of the absolute probability per VEI for the set of  
 413 potential analogues, which captures the spread of the data between the 25<sup>th</sup> and 75<sup>th</sup> percentile.  
 414 6. Calculate the total IQR by adding all  $IQR_j$ .  
 415 7. Optimise 10,000 vectors of weights to identify the set of weights that minimises the total IQR.

416 When the target volcano is well-studied and has comprehensive records, this approach can be modified  
 417 to identify the weights that maximise the similarity of the analogues' absolute probabilities to the target  
 418 volcano. We discarded this option for Melimoyu because it only has data to calculate the absolute  
 419 probability of VEI 5 eruptions, meaning that we would be aiming to find other data-limited volcanoes.

### 420 4.3 Analogue selection

421 The selection of analogues was made by assessing the dispersion in the absolute probability derived  
 422 from the potential analogues (Fig. 7) and applying criteria deemed as important by SERNAGEOMIN  
 423 and VB to estimate the  $f$ -M relationship for Melimoyu. A particular volcano had to meet the following  
 424 criteria to be considered an analogue of Melimoyu:

- 425 a) The volcano has confirmed Holocene eruptions with an assigned VEI in the VOTW (GVP,  
 426 2013) or LaMEVE database (Crosweller et al., 2012). Otherwise, the eruptive behaviour cannot  
 427 be evaluated.  
 428 b) The volcano is not categorised as frequently active (i.e., “confirmed to have erupted at some  
 429 point during at least 25 of the past 100 years (since 1921)” (GVP, 2013)) on the set of  
 430 noteworthy volcanoes of the GVP  
 431 ([https://volcano.si.edu/faq/index.cfm?question=eov\\_noteworthy](https://volcano.si.edu/faq/index.cfm?question=eov_noteworthy)). This criterion is especially  
 432 relevant for estimating the  $f$ -M relationship for Melimoyu since there is no evidence of  
 433 eruptions in the last 100 years. With this criterion, we may be excluding analogue volcanoes  
 434 that can be used for other purposes (e.g., retrieving eruption source parameters for hazard  
 435 modelling).

- 436 c) The volcano has records of large explosive Holocene eruptions ( $VEI \geq 4$ ) in the VOTW (GVP,  
 437 2013) or LaMEVE database (Crosweller et al., 2012).
- 438 d) The volcano has produced similar compositions to Melimoyu in the past. The GVP lists, in  
 439 order of descending abundance, the following rock types for Melimoyu: Andesite/Basaltic  
 440 Andesite, Dacite, and Basalt/ Picro-Basalt. Depending on the information available in the GVP,  
 441 if the volcano has data for:
- 442 • *Rock types 1, 2 and 3*: it must have at least two rock types in common with Melimoyu,  
 443 and the most abundant rock type must be intermediate or felsic.
  - 444 • *Rock types 1 and 2*: it must have both rock types in common with Melimoyu,  
 445 independently of the order, but the most abundant rock type must be intermediate or  
 446 felsic.
  - 447 • *Rock type 1*: it must be Andesite/Basaltic Andesite.

#### 448 4.4 Frequency-magnitude relationship

449 Once we had the selection of analogues for Melimoyu, we manually updated the start date for those  
 450 large magnitude eruptions ( $M \geq 4$ ) that had corrected dates in the latest version of LaMEVE (retrieved  
 451 17 August 2022) (Crosweller et al., 2012). We also included  $M \geq 4$  Holocene eruptions that were missing  
 452 in the VOTW database but available in the LaMEVE database.

453 The updated record of confirmed eruptions since the RCDs from the selection of analogue volcanoes  
 454 was used to re-calculate the absolute probability per VEI ( $P_{ABS}$ ). The sum of the absolute probabilities  
 455 per VEI from each analogue gives us the absolute probability of having an eruption of any VEI ( $P$ ) at a  
 456 given analogue volcano  $i$ :

$$457 \quad P_i = \sum_k P_{ABS \ ik} \quad (3)$$

458 Using the absolute probability, we calculated the conditional probability  $P_{COND}$  (i.e., the relative  
 459 probability of a given VEI  $j$ , conditional on an eruption occurring) per analogue volcano  $i$  as follows:

$$460 \quad P_{COND \ ij} = \frac{P_{ABS \ ij}}{\sum_k P_{ABS \ ik}} \quad (4),$$

461 where  $k$  indicates the VEI  $j$  with a  $P_{ABS \ ij} \neq 0$ .

462 The absolute and conditional probabilities from the set of analogues were used to estimate the  $f$ - $M$   
 463 relationship for Melimoyu as follows:

- 464 1. Model the empirical absolute probability  $P$  from the set of analogues by a Gamma  
 465 distribution, as proposed by Rodado et al. (2011) and Solow (2001), with parameters  $\alpha$   
 466

467 (shape) $>0$  and  $\lambda$  (rate) $>0$  estimated via maximum likelihood. The probability density  
 468 function of a gamma distribution is given by:

$$469 \quad f(x) = \begin{cases} \frac{\lambda x^{\alpha-1} e^{-\lambda x}}{\Gamma(\alpha)}, & x > 0 \\ 0, & x \leq 0 \end{cases} \quad (5)$$

470 We extract the 5<sup>th</sup>, 50<sup>th</sup>, and 95<sup>th</sup> percentiles from the Cumulative Distribution Function  
 471 (CDF), which reflects the uncertainty in the absolute probability for Melimoyu.

472 2. Quantify the variability in the conditional probability  $P_{COND}$  via bootstrapping with  
 473 replacement (i.e., a datapoint can be included more than once in a resampled dataset). From  
 474 the empirical conditional probabilities for  $n$  analogue volcanoes calculated from eq. 4, we  
 475 draw 5,000 bootstrap samples of size  $n$  and calculate the average conditional probability  
 476 per VEI from each resampled dataset. We extract the 5<sup>th</sup>, 50<sup>th</sup>, and 95<sup>th</sup> percentiles from the  
 477 marginal empirical CDF of the conditional probability for each VEI.

478 3. Calculate the absolute probability per VEI  $j$  for Melimoyu as follows:

$$479 \quad P_{ABSj} = P \times P_{CONDj}$$

## 480 5. Results

### 481 5.1 Analogues from the raw dataset

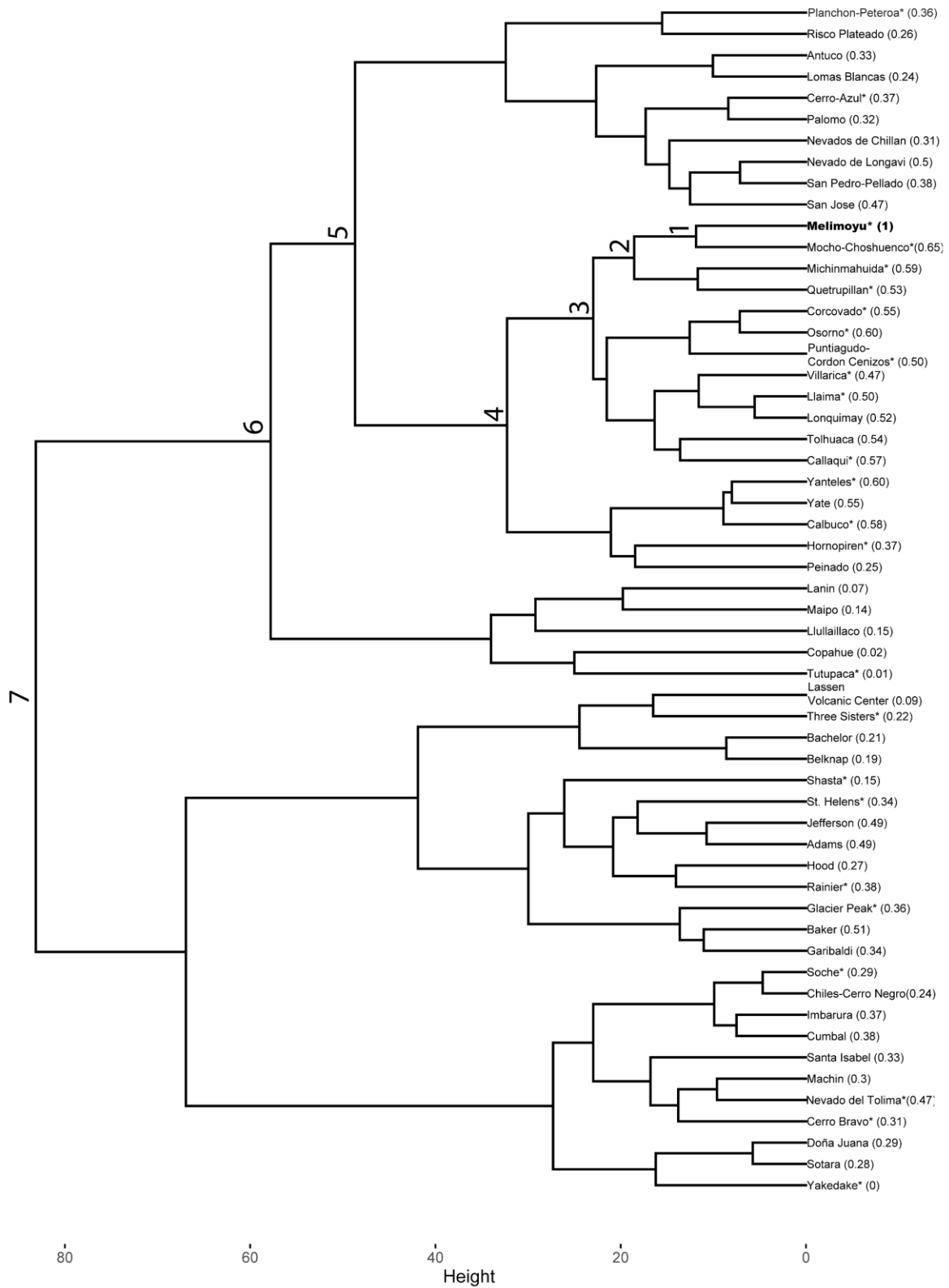
482 The agglomerative coefficient of the hierarchical clustering ranges from 0.778 for the single linkage  
 483 method to 0.949 for Ward's linkage method, indicating that the latter is the best linkage method. The  
 484 agglomerative coefficient close to 1 indicates a strong clustering structure in the dendrogram derived  
 485 from the raw dataset. This indication of good quality of the clustering is corroborated by the Hopkins  
 486 statistics (H) of 0.848, which indicates that the raw dataset is highly clusterable.

487 We cut the dendrogram at the minimum height that contains at least 50 volcanoes, approximately 80,  
 488 generating a set of 56 potential analogues, including Melimoyu (Fig. 2). Within this set of potential  
 489 analogues, we find seven nodes connected to Melimoyu's smaller cluster (Node 1), which indicate  
 490 different levels of similarity (i.e., the higher up in the tree the least similar to Node 1). Forty-two  
 491 potential analogues are in the region of South America, 13 in Canada and Western USA, and 1 in  
 492 Honshu (Japan).

493 Based on the normalised Manhattan distance shown in Figure 2 (i.e., the closer to 1, the more similar  
 494 to Melimoyu), Mocho-Choshuenco (Chile) is the most similar volcano to Melimoyu ( $M_{norm}=0.65$ ) and  
 495 therefore, the best analogue when using this method. The dendrogram captures this similarity since it



496 is the first volcano to be grouped with Melimoyu. Osorno, Yanteles, Michinmahuida, Calbuco, and  
 497 Callaqui, also located in Chile, follow closely with relatively similar distances.



498

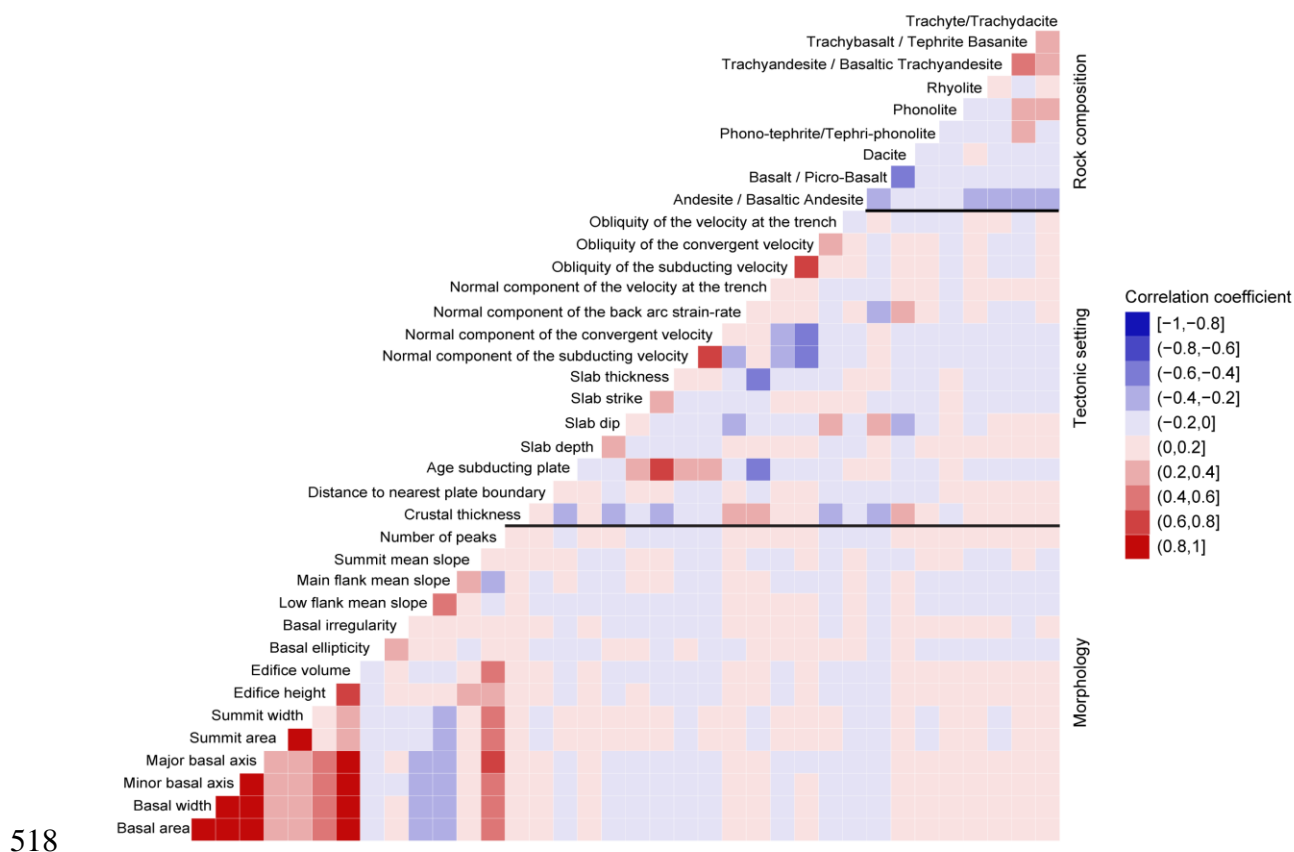
499 **Fig. 2.** Dendrogram generated from the application of AGNES using Ward's linkage method to the raw  
500 dataset. The value in parenthesis shows the normalised Manhattan distance ( $M_{\text{norm}}$ ). The closer  $M_{\text{norm}}$  is  
501 to 1, the most similar to Melimoyu (highlighted in bold). The node number indicates the different levels  
502 of similarity between a given cluster and the smaller cluster that contains Melimoyu (Node 1). The  
503 asterisk indicates if a volcano has  $\text{VEI} \geq 4$  Holocene eruptions records in the VOTW or LaMEVE  
504 database.

## 505 *5.2 Analogues from the reduced dataset*

506 Using Kendall's Tau correlation coefficient to assess the relationship between the variables, the  
507 correlation matrix shown in Figure 3 shows that several variables describing the morphology of the  
508 base and the summit's edifice are very strongly correlated. Since we aim to exclude redundant variables  
509 (i.e.,  $r \geq 0.8$ ), the following variables are not considered for the PCA: minor and major basal axis, basal  
510 width, basal area, and summit width.

511 Other variables with a strong positive correlation are the age of the subducting plate and slab thickness,  
512 normal convergent and subducting velocity components, and the convergent and subducting obliquity.  
513 For the rock composition, we observe that Trachy-Andesite/Basaltic Trachyandesite and  
514 Trachybasalt/Tephrite Basanite have a moderate positive correlation. In contrast, Basalt/Picro-Basalt  
515 and Dacite have a moderate negative correlation. Basalt/Picro-Basalt and Dacite also show a weak  
516 correlation with the crustal thickness, slab dip, and the normal component of the back arc strain-rate.

517



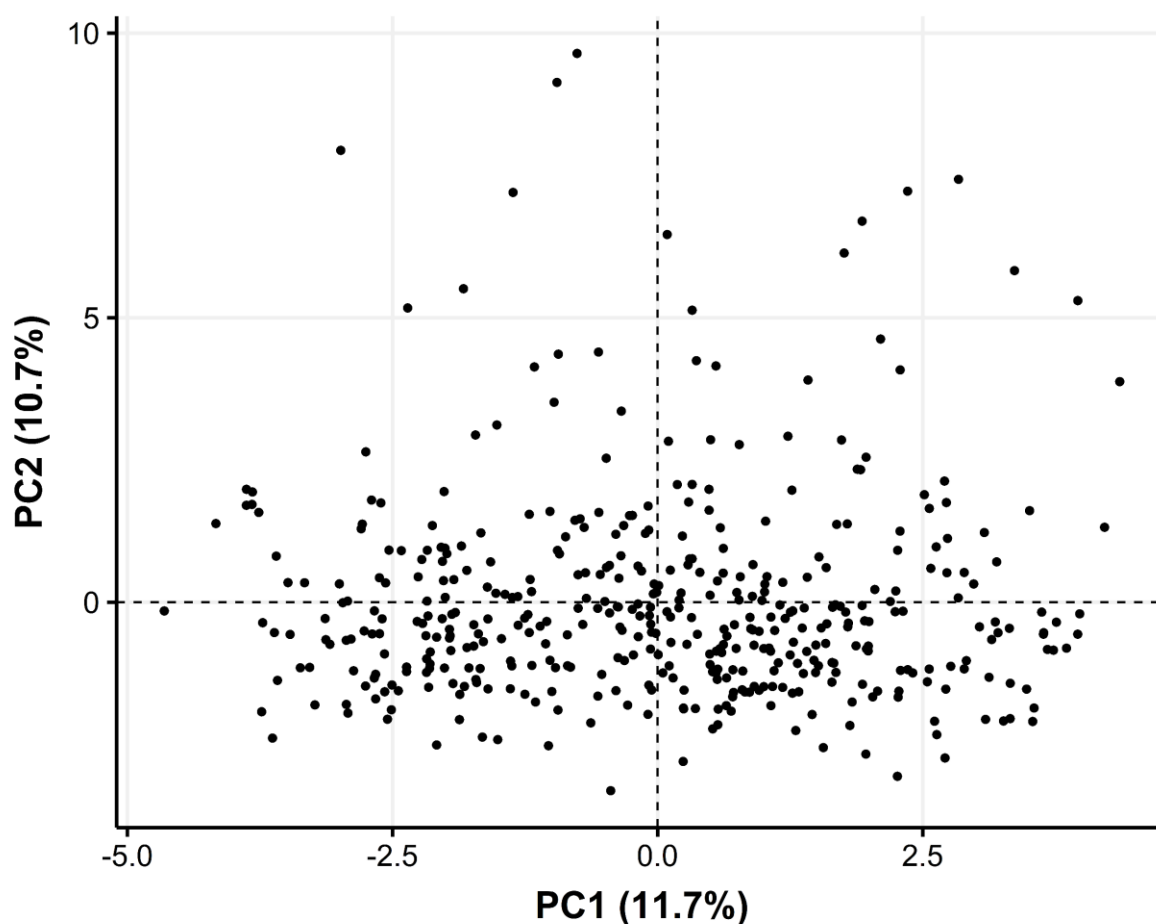
518

519 **Fig. 3.** Kendall's Tau correlation coefficient plot. Blue values indicate a negative correlation, and red  
 520 values a positive correlation. The variables are grouped into three main categories: morphology,  
 521 tectonic setting, and rock composition.

522 The standardised dataset of 32 variables (without redundant variables) was used as input for the PCA.  
 523 The results of the PCA show that the first two components explain around 22% of the variance (Fig. 4).  
 524 We require 11 PCs to capture at least 70% of the variance, which is one of the commonly used thresholds  
 525 in PCA (Jolliffe and Cadima, 2016). Furthermore, the 11 PCs have an eigenvalue (i.e., variance retained  
 526 by each PC) higher than one, indicating that they account for more variance than the original variables.  
 527 The new spatial projection (Fig. 4) does not show any obvious spatial clusters of volcanoes, which can  
 528 be due to the low variance retained by PC 1 and 2. A low variance in the main PCs could indicate that  
 529 our dataset does not lie within a two-dimensional linear subspace. One solution we explored was using  
 530 non-linear dimensionality reduction techniques (e.g., UMAP; (McInnes et al., 2020)). However, these  
 531 techniques required tuning hyper-parameters by looking at how the data is distributed in the space,  
 532 leading to a biased selection that could influence the clustering results.

533 Table 1 shows the percentage with which each variable contributes to explaining the variability in each  
 534 PC (e.g., the age of the subducting plate explains ~17% of the variability in PC1). We observe that  
 535 variables describing the tectonic setting (e.g., age of the subducting plate, slab thickness, normal  
 536 component of the subducting velocity, crustal thickness, and obliquity of the subducting velocity)

537 contribute the most in accounting for the variability in PC1. In contrast, variables describing the volcano  
 538 morphology (e.g., edifice volume, number of peaks, summit area, low flank mean slope, and main flank  
 539 mean slope) have the highest contributions in PC2. Lastly, we observe that the composition contributes  
 540 more to the later PCs.



541  
 542 **Fig. 4.** Representation of individual volcanoes projected in the PC1 and PC2. The value in parentheses  
 543 indicates the percentage of explained variance by that PC.

544 **Table 1.** Variable contribution (%) of each variable to explain the variability for the 11 PCs retained  
 545 for the analysis. The value in parentheses in the first row indicates the percentage of explained variance  
 546 by that PC. Values in bold indicate the top 5 variables with the higher contribution to each PC. Variables  
 547 are grouped by category and ordered by descending contribution in PC 1.

	Variables	PC1 (11.7%)	PC2 (10.7%)	PC3 (8.9%)	PC4 (7.8%)	PC5 (6.2%)	PC6 (5.5%)	PC7 (4.8%)	PC8 (4.2%)	PC9 (3.9%)	PC10 (3.6%)	PC11 (3.5%)
Tectoni c	Age of the subducting plate	<b>17.07</b>	0.55	0.01	5.56	0.27	3.01	0.04	0.37	0.05	2.37	0.42
	Thickness of the slab	<b>14.67</b>	0.56	1.38	<b>8.23</b>	0.36	2.55	0.22	1.11	0.01	1.94	0.34

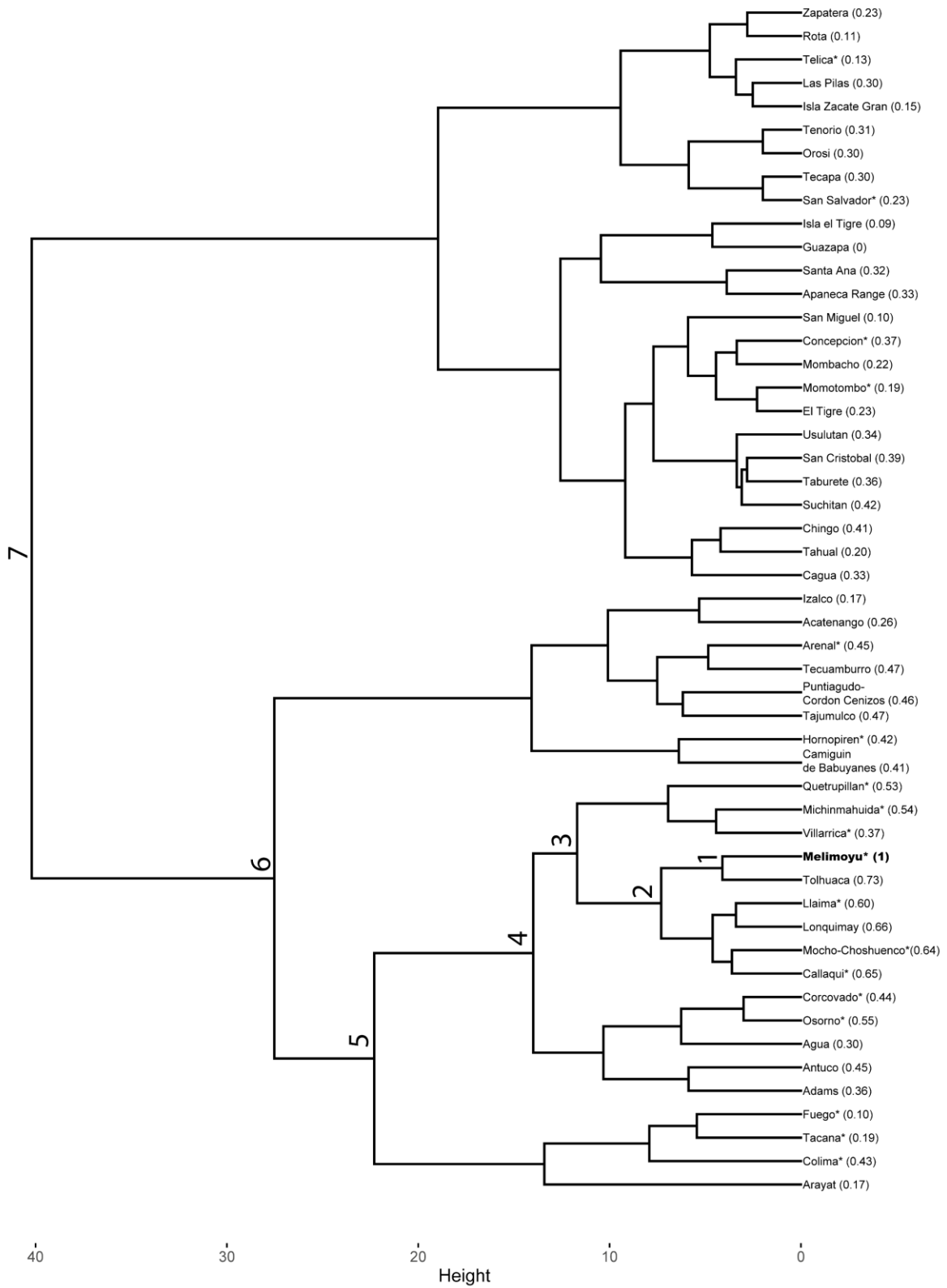
Rock composition	Normal component of the subducting velocity	<b>8.9</b>	0.12	5.38	<b>9.91</b>	1.59	0.18	<b>5.52</b>	0.16	0.93	0	0.04
	Crustal thickness	<b>7.85</b>	0.13	<b>11.03</b>	0.9	0.53	2.62	1.83	0.39	0.02	0.65	0.07
	Obliquity of the subducting velocity	<b>7.75</b>	0.39	<b>11.2</b>	0.46	0.64	2.01	0.03	0.19	0.2	0.37	<b>6.39</b>
	Obliquity of the convergent velocity	7.1	0.31	<b>16.09</b>	0.15	1.46	1.28	0.9	0	0.07	0.05	1.1
	Normal component of the convergent velocity	5.1	0.47	<b>14.22</b>	0.83	0.56	0.74	3.01	0.11	0.02	0	0.55
	Normal component of the velocity at the trench	3.96	0.3	4.12	<b>16.07</b>	0.61	0.28	3.09	0	0.84	0.7	1.8
	Strike of the slab	3.41	0.6	1.86	3.99	1.32	0.73	1	3.43	2.46	3.74	0
	Normal component of the back arc strain-rate	1.7	0.13	1.02	7.97	5.62	1.43	<b>21.17</b>	0.03	1.24	0	1.31
	Obliquity of the velocity at the trench	1.08	0.01	<b>12.34</b>	1.42	0.25	4.69	0.05	0.05	1.63	0.17	2.55
	Dip of the slab	0.88	3.46	7.95	2.37	4.03	<b>11.81</b>	0.22	1.83	0.19	1.61	2.04
	Depth of the slab	0.13	6.6	0.06	0.23	5.49	0.54	1.49	<b>11.86</b>	1.58	0.11	1.21
	Distance to nearest plate boundary	0.02	0.55	0.26	<b>8.23</b>	2.1	4.1	1.7	0	2.7	<b>4.78</b>	0.21
	Basalt / Picro-Basalt	5.26	2.8	1.74	1.91	4.11	3.62	1.92	<b>6.54</b>	0.12	1.6	<b>8.9</b>
	Rhyolite	0.69	0.11	0.06	0.07	0.01	0.16	2.01	1.02	<b>8.29</b>	<b>19.8</b>	<b>31.81</b>
	Trachyte/Trachydacite	0.53	1.94	0.01	0.01	4.53	<b>10.1</b>	1.27	0.59	<b>13.95</b>	1.71	0.59
	Phonotephrite/Tephriphonolite	0.31	0.29	0.05	0.01	1.91	1.73	5.38	2.64	<b>39.67</b>	1.96	<b>5.81</b>
Trachyandesite / Basaltic Trachyandesite	0.16	2.79	0.02	0	<b>8.06</b>	3.9	3	1.24	<b>6.48</b>	0.46	3.19	
Andesite / Basaltic Andesite	0.12	5.77	0	1.5	<b>7.33</b>	1.74	1.02	6.47	1.69	<b>30.59</b>	2.43	
Trachybasalt / Tephrite Basanite	0.07	5.11	0.07	0.17	<b>8.7</b>	<b>7.34</b>	<b>9.46</b>	0.14	<b>10.49</b>	0.29	1	
Phonolite	0.03	1.01	0.01	0.62	3.69	2.78	1.52	<b>10.04</b>	1.8	1.25	5.17	
Morphology	Basal irregularity	3.1	0.83	1.79	0	2.35	0.13	2.88	<b>14.29</b>	0.04	0.67	3.84
	Edifice height	1.81	1.24	2.87	<b>8.52</b>	0.01	<b>6</b>	<b>8.96</b>	3.59	1.62	0.05	0.05
	Low flank mean slope	0.82	<b>10.16</b>	1.19	0.28	2.41	3.5	4.1	1.51	0.02	4.45	<b>8.49</b>
	Number of peaks	0.56	<b>13.2</b>	0.55	2.33	3.93	3.21	0.17	3.93	0.35	1.23	0.3
	Edifice volume	0.48	<b>13.39</b>	1.14	4.68	4.62	4.44	4.03	0.02	0.03	0.42	1.04
	Summit mean slope	0.2	1.61	0.28	5.82	4.5	<b>7.81</b>	5.25	0.16	2.11	0.01	4.21
	Main flank mean slope	0.06	<b>11.57</b>	1.14	0.57	<b>6.94</b>	5.23	<b>7.28</b>	0.01	0.59	1.78	2.38
	Basal ellipticity	0.04	0.12	0	6.56	0.29	0.05	0.12	<b>26.64</b>	0.36	<b>5.15</b>	1.56
	Summit area	0.03	<b>12.67</b>	0	0.56	<b>8.17</b>	0.65	0.43	1.02	0.29	1.72	0.42

548

549 The reduced dataset containing the coordinates of 438 volcanoes at the 11 PCs was used as input data  
550 for AGNES. The agglomerative coefficient ranges from 0.885 for single linkage method to 0.944 for  
551 Ward's linkage method. As we did for the raw dataset, we select the hierarchical clustering results from

552 Ward's linkage method since it generates the strongest clustering structure. In addition, the Hopkins  
553 statistic ( $H=0.836$ ) indicates that the reduced dataset is highly clusterable.

554 We cut the resulting dendrogram (Fig. 5) at an approximate height of 40, producing a cluster of 51  
555 volcanoes, including Melimoyu. This dendrogram contains groups of volcanoes with seven different  
556 levels of similarity relative to the smaller cluster containing Melimoyu (Node 1). Twenty-one potential  
557 analogues are in the region of Mexico, Guatemala, Nicaragua, Costa Rica, and Panama; 14 in South  
558 America; 13 in El Salvador and Honduras; 2 in Luzon; 1 in North Luzon, Central Philippines,  
559 Mindanao, and SE Asia; and 1 in Canada and Western USA. The volcano with the highest normalised  
560 Manhattan distance (i.e., best analogue) ( $M_{\text{norm}}=0.73$ ) is Tolhuaca (Chile). Other volcanoes with  
561 relatively high distance values (e.g.,  $M_{\text{norm}}=0.60-0.66$ ) are Lonquimay, Callaqui, Mocho-Choshuenco,  
562 and Llaima.



563

564 **Fig. 5.** Cut dendrogram generated from the application of AGNES using Ward's linkage method to the  
 565 reduced dataset. The value in parenthesis shows the normalised Manhattan distance ( $M_{norm}$ ). The closer

566  $M_{\text{norm}}$  is to 1, the most similar to Melimoyu (highlighted in bold). The node number indicates the  
567 different levels of similarity between a given cluster and the smaller cluster that contains Melimoyu  
568 (Node 1). The asterisk indicates if a volcano has  $\text{VEI} \geq 4$  Holocene eruptions records in the VOTW or  
569 LaMEVE database.

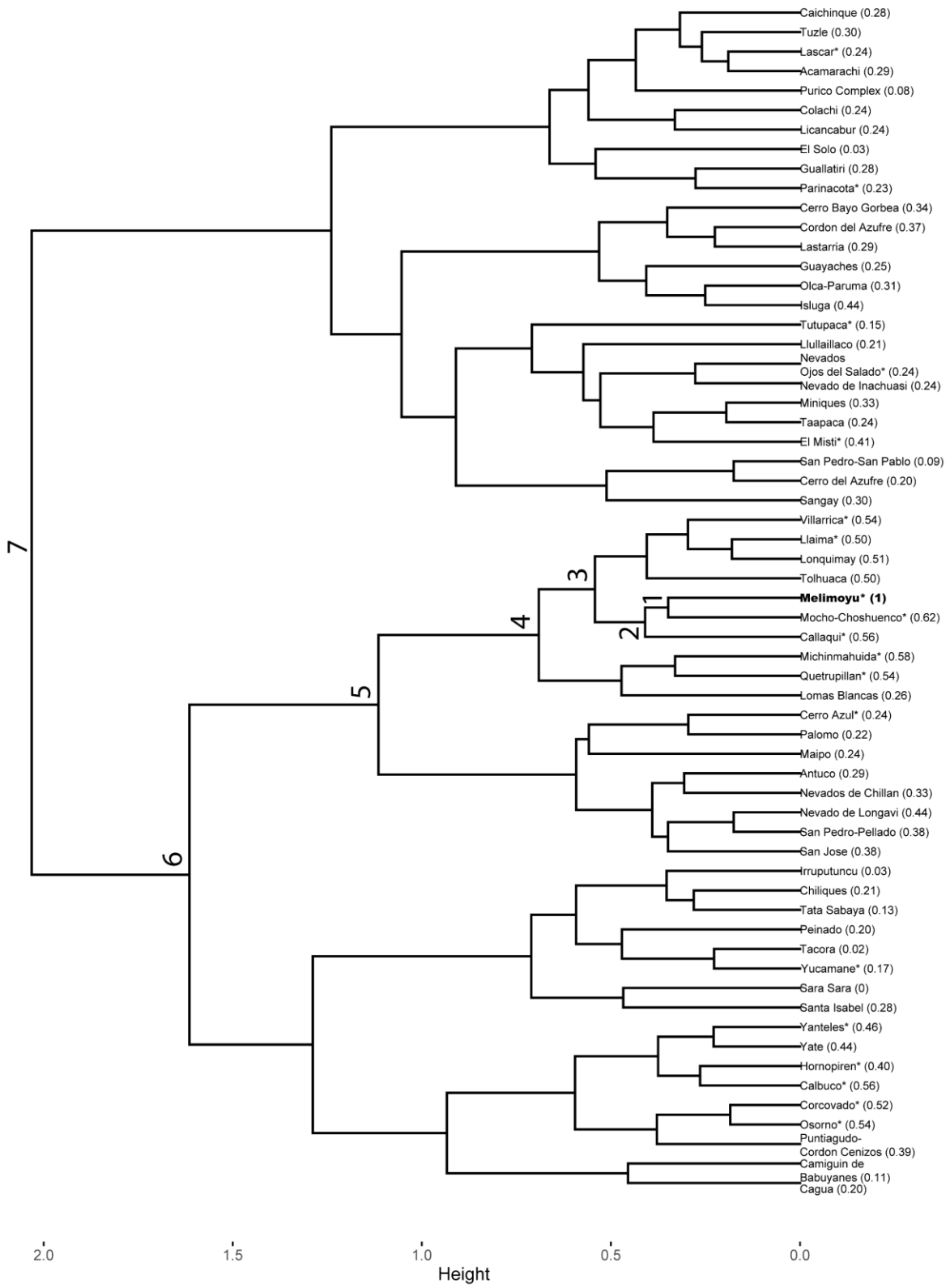
### 570 *5.3 Analogues from the weighted dataset*

571 To optimize the set of weights that minimise the spread in calculated absolute eruption probabilities  
572 across the set of analogues, we first need to account for the completeness of the eruption record. The  
573 most complete portion of the VOTW database was identified by calculating regional RCDs as a function  
574 of  $\text{VEI} \leq 1, 2, 3, 4,$  and  $\geq 5$  using the change point method from Burgos et al. (2022b). The RCDs  
575 (supplementary material 3) define the time windows required for absolute probabilities for the set of  
576 potential analogues. The resulting RCDs range from a few centuries (e.g., 1979 for VEI 3 eruptions in  
577 Africa (northern, western, central)) to thousands of years (e.g., 4700 BCE for VEI 4 eruptions in New  
578 Zealand), and they are highly variable across regions and eruption sizes.

579 We use Ward's linkage method, which produced the highest agglomerative coefficients in the previous  
580 two datasets, instead of testing the four linkage methods to reduce the computation time in optimising  
581 the weighting scheme. The complete set of weights that generates the set of analogues with the lowest  
582 total IQR (0.01214) is available in supplementary material 4. Another 11 weighting schemes that can  
583 also be found in supplementary material 4 produce similar IQR (0.1224). We will focus on the results  
584 derived from the weighting scheme that produces the lowest IQR. We observe that the three most  
585 'important' variables (i.e., top 3 highest weights) are the obliquity of the velocity at the trench, the basal  
586 irregularity, and the normal component of the convergent velocity.

587 The dendrogram obtained from the weighted dataset has an agglomerative coefficient of 0.947 and a  
588 Hopkins statistic of 0.833, indicating a strong clustering. We cut the dendrogram at an approximate  
589 height of 2 generating a set of 61 volcanoes, including Melimoyu (Fig. 6). We find seven levels of  
590 similarity relative to the smaller cluster containing Melimoyu (Node 1). Fifty-nine potential analogues  
591 are in the region of South America; 1 in Luzon; and 1 in North Luzon, Central Philippines, Mindanao,  
592 and SE Asia. The most similar volcano based on the normalised distance metric is Mocho-Choshuenco  
593 ( $M_{\text{norm}} = 0.62$ ). Other similar volcanoes are Michinmahuida, Callaqui, Calbuco, and Osorno, with a  
594 normalised distance ranging from 0.54 to 0.58.





595

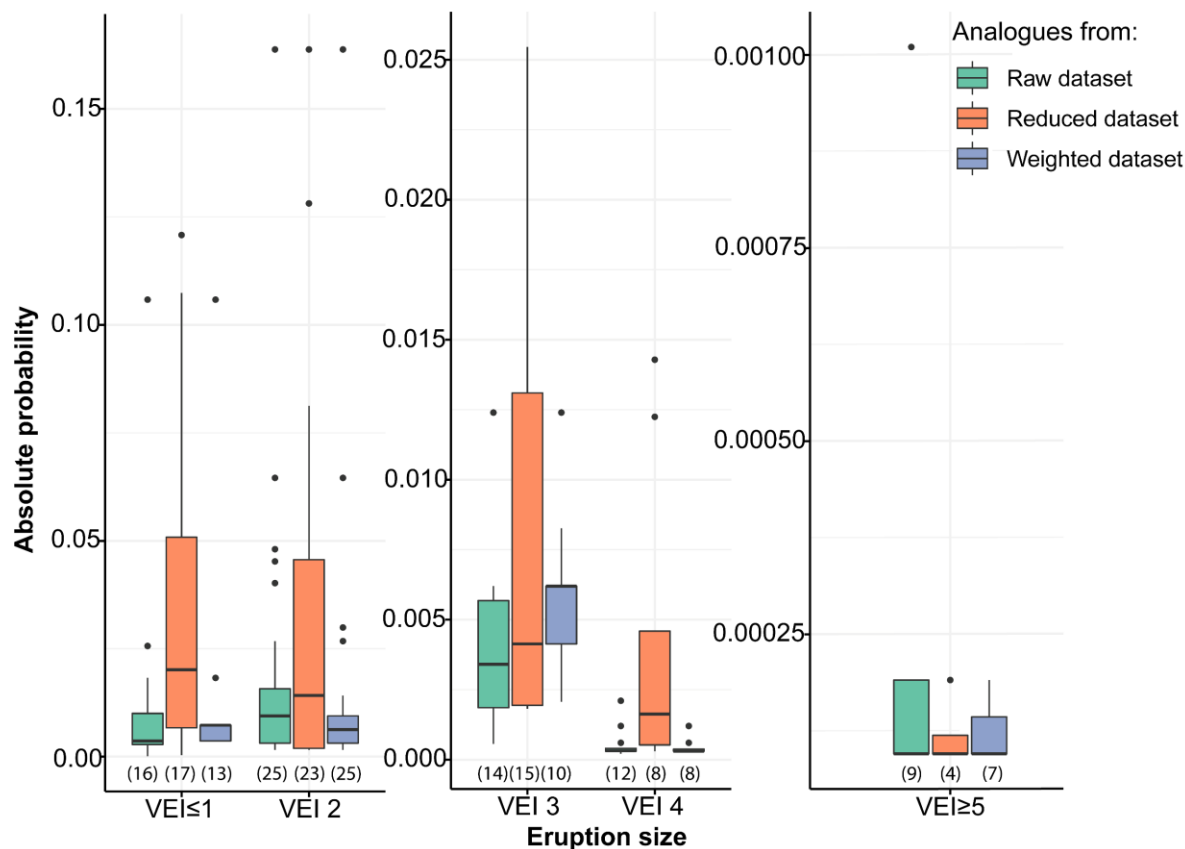
596

597 **Fig. 6.** Cut dendrogram generated from the application of AGNES using Ward's linkage method to the  
598 weighted dataset. The value in parenthesis shows the normalised Manhattan distance ( $M_{\text{norm}}$ ). The closer  
599  $M_{\text{norm}}$  is to 1, the most similar to Melimoyu (highlighted in bold). The node number indicates the  
600 different levels of similarity between a given cluster and the smaller cluster that contains Melimoyu  
601 (Node 1). The asterisk indicates if a volcano has  $\text{VEI} \geq 4$  Holocene eruptions records in the VOTW or  
602 LaMEVE database.

#### 603 *5.4 Analogue selection for Melimoyu*

604 The sensitivity analysis shows that the quality of the results, in terms of clustering performance, is very  
605 similar for the three datasets, with slightly higher values of the agglomerative coefficient and Hopkins  
606 statistic for the raw dataset. In the three cases, these internal validation metrics indicate inherent  
607 clustering in the data and a strong clustering structure in the dendrograms. These results were obtained  
608 using Ward's linkage method, which groups clusters with minimum total-within variance, known for  
609 its tendency to produce compact clusters (Kaufman and Rousseeuw, 1991).

610 As a first step for selecting the analogues for Melimoyu, we analyse the dispersion in the absolute  
611 probabilities estimated from each set of potential analogues (Fig. 2, 5, and 6). The dispersion in the  
612 absolute probability shown in Figure 7 informs us about the difference in the eruptive behaviour  
613 between the volcanoes in the three sets of potential analogues. The absolute probabilities for all the  
614 potential analogues generated from the three different input datasets can be found in supplementary  
615 material 5. As expected, the set of potential analogues derived from the weighted dataset, which was  
616 tuned to obtain the lowest aggregate IQR, produced lower uncertainties, except for  $\text{VEI} \geq 5$  eruptions. In  
617 contrast, the set of analogues from the reduced dataset produced the most dispersed absolute  
618 probabilities, indicating that the volcanoes proposed as analogues have notably different recurrence  
619 rates per VEI class. Meanwhile, the dispersion from the analogues derived from the raw dataset is  
620 between that of the other two datasets. We observe that the absolute probability decreases with the  
621 eruption size, with a difference of several orders of magnitude between some volcanoes with  $\text{VEI} \leq 1$   
622 and  $\text{VEI} \geq 5$ .



623

624 **Fig. 7.** Comparison of the absolute annual probability ( $p_{ij}$ ) per VEI for the three sets of potential  
 625 volcanoes derived from the raw, reduced, and weighted dataset. The number in parentheses below the  
 626 boxplots indicates the number of data points (i.e., the number of volcanoes with at least one eruption of  
 627 a given VEI within the complete portion of the record in supplementary material 3). Note: y-axes are in  
 628 different scales.

629 After analysing the dispersion in Figure 7, we apply the criteria for being an analogue of Melimoyu  
 630 (Section 4.3). In addition to Melimoyu, we find that 20 out of 55 volcanoes, 8 out of 50 volcanoes, and  
 631 13 out of 60 volcanoes obtained from the raw dataset, reduced dataset, and weighted dataset,  
 632 respectively, meet these criteria (see supplementary material 5 for the three lists of potential analogues).

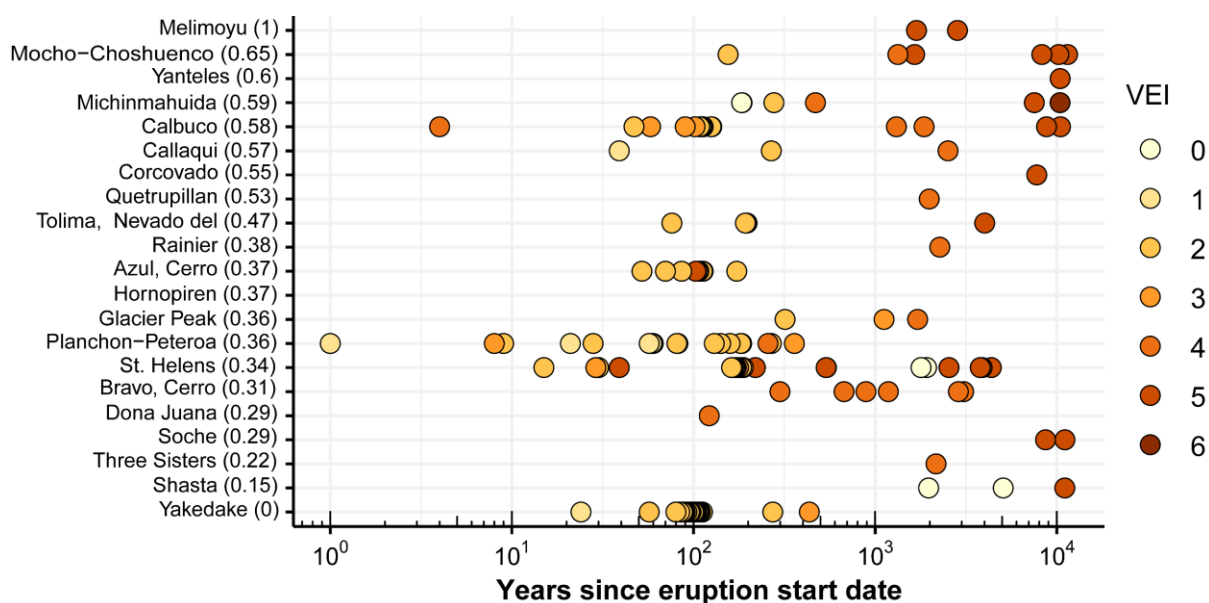
633 Due to the large dispersion in the absolute probability and the low number of volcanoes meeting the  
 634 criteria, we discard the set of potential analogues derived from the reduced dataset. The other two sets  
 635 of potential analogues have a similar range of absolute probabilities, although the dispersion is slightly  
 636 lower for the analogues derived from the weighted dataset (Fig. 7). However, more volcanoes derived  
 637 from the raw database meet the criteria for being analogues. Therefore, we retain the results from the  
 638 raw dataset and conclude that it contains the best selection of analogues to calculate the empirical  $f$ - $M$   
 639 relationship for Melimoyu.

640 The selection of 20 analogues that meet the criteria, ordered from more to less similar (i.e., highest to  
 641 lowest normalised Manhattan distance in Figure 8), are Mocho-Choshuenco, Yanteles, Michinmahuida,

642 Calbuco, Callaqui, Corcovado, Quetrupillán, Nevado del Tolima, Rainier, Cerro Azul, Hornopirén,  
 643 Glacier Peak, Planchón-Peteroa, St. Helens, Cerro Bravo, Doña Juana, Soche, Three Sisters, Shasta,  
 644 and Yakedake. These volcanoes are located in the regions of South America (n=14), Canada and  
 645 Western USA (n=5), and Honshu (n=1).

646 *5.5 Eruption probabilities for Melimoyu*

647 The eruption records from the selection of analogues derived from the raw dataset are used to calculate  
 648 the empirical  $f$ - $M$  relationship (Fig. 8). All the 20 analogues, except for Hornopirén, have at least one  
 649 confirmed eruption within the complete portion of the eruption record (i.e., since the RCD in Table 2).  
 650 From a total of 133 eruptions produced by all these volcanoes since the regional RCDs, nine eruptions  
 651 missing in the VOTW database were added from LaMEVE, and the start date from 11 eruptions was  
 652 updated with the corrected radiocarbon dates from LaMEVE. As a result of these modifications, we  
 653 changed the RCD for  $VEI \geq 5$  eruptions in South America, which was defined as the oldest eruption in  
 654 the region (i.e., from -8460 to -9941). Therefore, the  $VEI \geq 5$  absolute probabilities estimated for  
 655 volcanoes in South America are slightly higher than those estimated with the updated RCD (e.g.,  $1.9 \times 10^{-4}$   
 656 vs  $1.7 \times 10^{-4}$  for Michinmahuida in tabs ‘Analogues raw dataset’ and ‘Analogue selection’ in  
 657 supplementary material 5).



658  
 659 **Fig. 8.** Confirmed eruptions within the most complete eruption record from the analogue selection.  
 660 These data were used for estimating the absolute and conditional probabilities in Figure 9. Volcanoes  
 661 are listed in descending order of  $M_{norm}$  in parenthesis (i.e., more to less similar to Melimoyu). The origin  
 662 of the x-axis (i.e., zero years) corresponds to 2019.

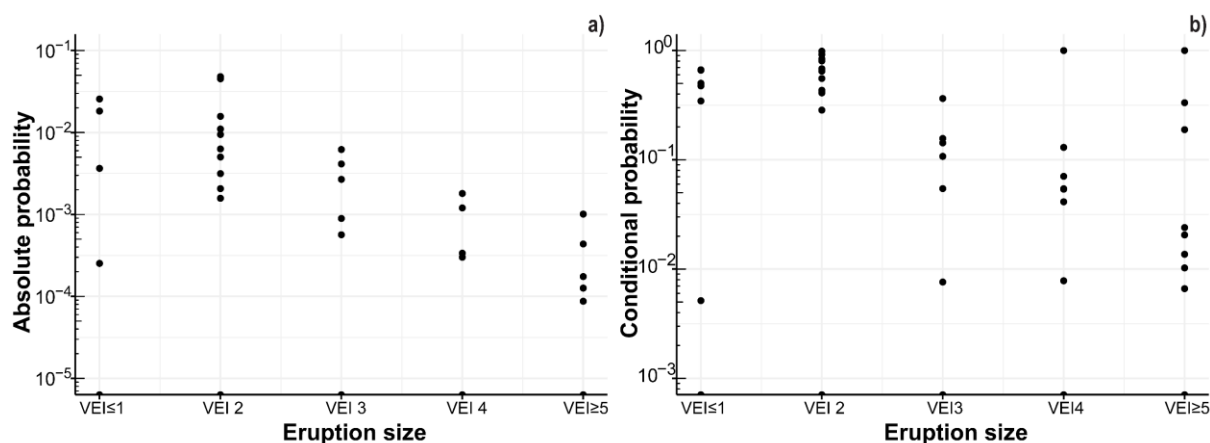
663 **Table 2.** Relative Completeness Dates (RCDs) used to calculate the probabilities in Figure 8. Dates in  
 664 regular font indicate that the RCD corresponds to the most abrupt change point, dates in cursive indicate

665 that the RCD corresponds to the oldest eruption, and dates with an asterisk in cursive indicate that the  
 666 RCD correspond to an alternative change point. See Burgos et al. (2022b) for method.

Region	VEI $\leq$ 1	VEI 2	VEI 3	VEI 4	VEI $\geq$ 5
Canada and Western USA	-5890	1820	900	-950	-5900
South America	1745*	1384	1535	-1310	-9941
Honshu	1863	1582	250	-2750	-8250

667

668 The eruption record presented in Figure 8 and the RCDs in Table 2 were used to estimate the absolute  
 669 and conditional probability for each analogue (Fig. 9). We observe that, with the exception of VEI $\leq$ 1,  
 670 the absolute probability decreases as the eruption size increases (Fig. 9a). The absolute probability  
 671 varies up to one order of magnitude between analogues, except for VEI $\leq$ 1 and VEI 5 eruptions, which  
 672 vary up to two orders of magnitude. Following the trend observed in Fig 9a, the overall range of  
 673 conditional probabilities decreases for larger VEIs (Fig. 9b). We observe that several volcanoes, such  
 674 as Corcovado, have a 100% conditional probability of VEI 4 or VEI $\geq$ 5 eruptions because they do not  
 675 have records from other eruption sizes within the complete portion of the catalogue (Fig. 8).



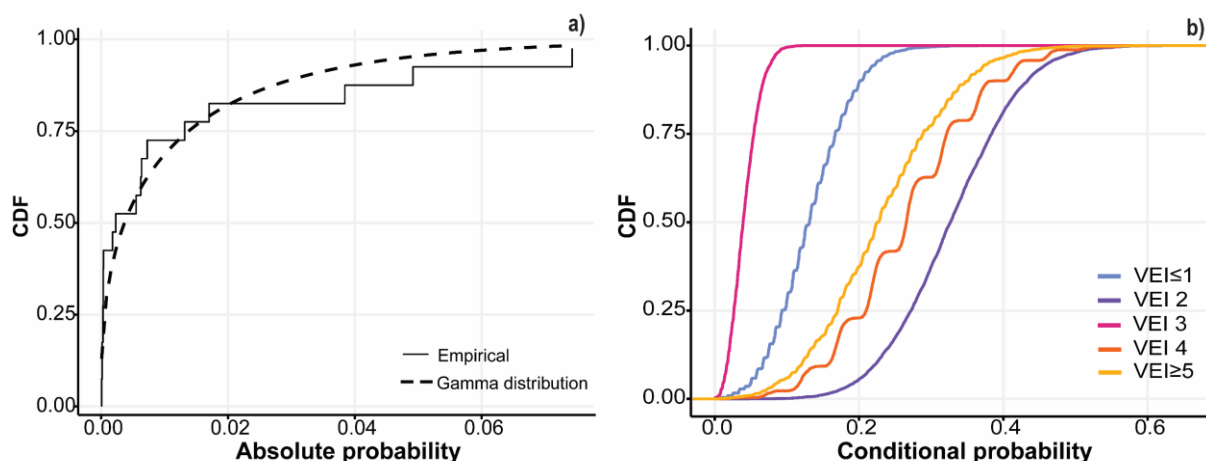
676

677 **Fig. 9.** Absolute (a) and conditional probability (b) per VEI from each volcano in the analogue selection  
 678 with eruption data within the complete portion of the catalogue. The number of data points for VEI $\leq$ 1,  
 679 2, 3, 4, and  $\geq$ 5 is 6, 10, 6, 11, and 11, respectively.

680 The  $f$ - $M$  relationship and eruption probability estimate for Melimoyu is shown in Figure 10 and Table  
 681 3. The absolute probability of having an eruption of any VEI at Melimoyu can be modelled by the  
 682 gamma distribution in Figure 10a with shape parameter ( $\alpha$ ) 0.369 and rate ( $\beta$ ) 32.96. The 5<sup>th</sup>, 50<sup>th</sup>, and  
 683 95<sup>th</sup> percentiles extracted from the CDF give an absolute probability of  $6.55 \times 10^{-6}$ ,  $3.68 \times 10^{-3}$ , and  
 684  $4.78 \times 10^{-2}$ , respectively. The low value of the median probability (i.e., on average, one eruption every  
 685 272 years) reflects the low frequency of eruptions at Melimoyu, indicating that long periods of  
 686 dormancy are common across the selection of analogues.

687 Meanwhile, the empirical CDFs in Figure 10b derived from bootstrap sampling show that the median  
 688 conditional probability is the highest for VEI 2 eruptions, likely because it is the default value assigned  
 689 in the VOTW database to explosive eruption without detailed descriptions (Siebert et al., 2011). The  
 690 lowest conditional probabilities correspond to VEI 3 followed by  $VEI \leq 1$ , which might be explained by  
 691 the lower number of volcanoes ( $n=6$ ) with records from eruptions of these sizes. Assuming that an  
 692 eruption occurs at Melimoyu, there is a 49% probability that the VEI is equal to or larger than four (50<sup>th</sup>  
 693 percentile of the conditional probability) (Table 3). The distribution of the conditional probabilities  
 694 derived from the analogue volcanoes captures the tendency to produce large explosive eruptions at  
 695 Melimoyu.

696 By multiplying the absolute and conditional probability, we obtain the absolute probability of an  
 697 eruption of a given VEI, which ranges from  $1.45 \times 10^{-4}$  for VEI 3 eruptions to  $1.2 \times 10^{-3}$  for VEI 2 eruptions  
 698 (Table 3). The absolute probability for VEI 4 and  $VEI \geq 5$  eruptions is similar, with a median average  
 699 recurrence interval given by the inverse of the absolute probability of 1024 and 1204 years, respectively.



700  
 701 **Fig. 10.** Cumulative Distribution Function (CDF) of the absolute probability of an eruption of any VEI  
 702 (a) and empirical CDF of the conditional probability of a VEI given there is an eruption (b).

703  
 704 **Table 3.** Conditional and absolute probability of having an eruption of a given VEI at Melimoyu.

Eruption size	Conditional probability	Absolute probability
	50 <sup>th</sup> percentile [5 <sup>th</sup> ,95 <sup>th</sup> ]	50 <sup>th</sup> percentile [5 <sup>th</sup> ,95 <sup>th</sup> ]
$VEI \leq 1$	$1.31 \times 10^{-1}$ [ $5.06 \times 10^{-2}$ , $2.23 \times 10^{-1}$ ]	$4.82 \times 10^{-4}$ [ $3.32 \times 10^{-7}$ , $1.07 \times 10^{-2}$ ]
VEI 2	$3.27 \times 10^{-1}$	$1.20 \times 10^{-3}$

	$[1.97 \times 10^{-1}, 4.62 \times 10^{-1}]$	$[1.29 \times 10^{-6}, 2.21 \times 10^{-2}]$
	$3.93 \times 10^{-2}$	$1.45 \times 10^{-4}$
VEI 3	$[1.29 \times 10^{-2}, 7.78 \times 10^{-2}]$	$[8.45 \times 10^{-8}, 3.72 \times 10^{-3}]$
	$2.66 \times 10^{-1}$	$9.77 \times 10^{-4}$
VEI 4	$[1.19 \times 10^{-1}, 4.22 \times 10^{-1}]$	$[7.81 \times 10^{-7}, 2.02 \times 10^{-2}]$
	$2.26 \times 10^{-1}$	$8.30 \times 10^{-4}$
VEI $\geq$ 5	$[8.99 \times 10^{-2}, 3.79 \times 10^{-1}]$	$[5.89 \times 10^{-7}, 1.81 \times 10^{-2}]$

## 705 6. Discussion

### 706 6.1. Data availability

707 One limitation of hierarchical clustering is that it does not allow for missing values in the input data,  
 708 limiting our application to complete cases (i.e., we only include volcanoes without missing data for the  
 709 selected variables). Therefore, the variables and number of potential analogues used as input in the  
 710 clustering are limited by the available data for each volcano. For example, when searching analogues  
 711 for Melimoyu, only volcanoes in subduction zones are considered potential analogues since we include  
 712 variables in the clustering that are only descriptive of this tectonic setting (e.g., the geometry of the  
 713 slab). This is not considered a significant limitation in this study since the tectonic setting plays a key  
 714 role in factors such as the magma budget, plumbing system configuration, and the rock composition,  
 715 which partly controls the eruption style and recurrence in volcanic arcs (Acocella, 2014; Sheldrake and  
 716 Caricchi, 2017; Sheldrake et al., 2020; Weber and Sheldrake, 2022). Similarly, the morphometric  
 717 variables included in the global database are available only for shields, calderas, and composite  
 718 volcanoes (Grosse et al., 2014; Grosse and Kervyn, 2018). Other volcano types are not included in the  
 719 analysis, even though composite volcanoes, like Melimoyu, often have secondary volcanic features,  
 720 such as parasitic cones and fissures. Unfortunately, these secondary features are rarely characterised  
 721 and not included in global databases.

722 Not considering volcanoes in other tectonic settings or with different morphologies does not mean that  
 723 they cannot be analogues of Melimoyu. These volcanoes could have been included in the clustering at  
 724 the expense of excluding numerical variables that capture the variability across volcanoes within  
 725 subduction zones and across composite and shield volcanoes. However, increasing the number of  
 726 volcanoes included in the input data implies reducing the number of input variables since few are  
 727 available across all volcanoes. For example, only the primary volcano type and tectonic setting from  
 728 the VOTW database (GVP, 2013), which are categorical variables, the crustal thickness from Laske et  
 729 al. (2013), and the distance to plate boundaries from Bird (2003) are available for the 1428 volcanoes  
 730 listed in the global database. Even the variable rock type 1 from the VOTW database is missing for 76  
 731 out of 1428, meaning that rock composition would not be considered in the clustering if we included

732 all the volcanoes. A potential solution would be to identify the input dataset that maximises the number  
733 of variables and volcanoes.

734 The flexibility of AGNES and the straightforward application allow us to adjust the variables based on  
735 the available data for future applications of this approach to other target volcanoes. The number of  
736 variables for target volcanoes with data mostly limited to categorical information can be increased by  
737 transforming these variables into numerical variables via one-hot encoding or gathering new data (e.g.,  
738 spreading rate for mid-ocean ridges or morphometric parameters for other volcano types). Alternatively,  
739 other clustering algorithms that allow combining categorical and numerical variables could be tested  
740 (e.g., k-prototypes), although they require pre-defining the number of clusters, adding another level of  
741 iteration.

## 742 *6.2. Analogue suitability*

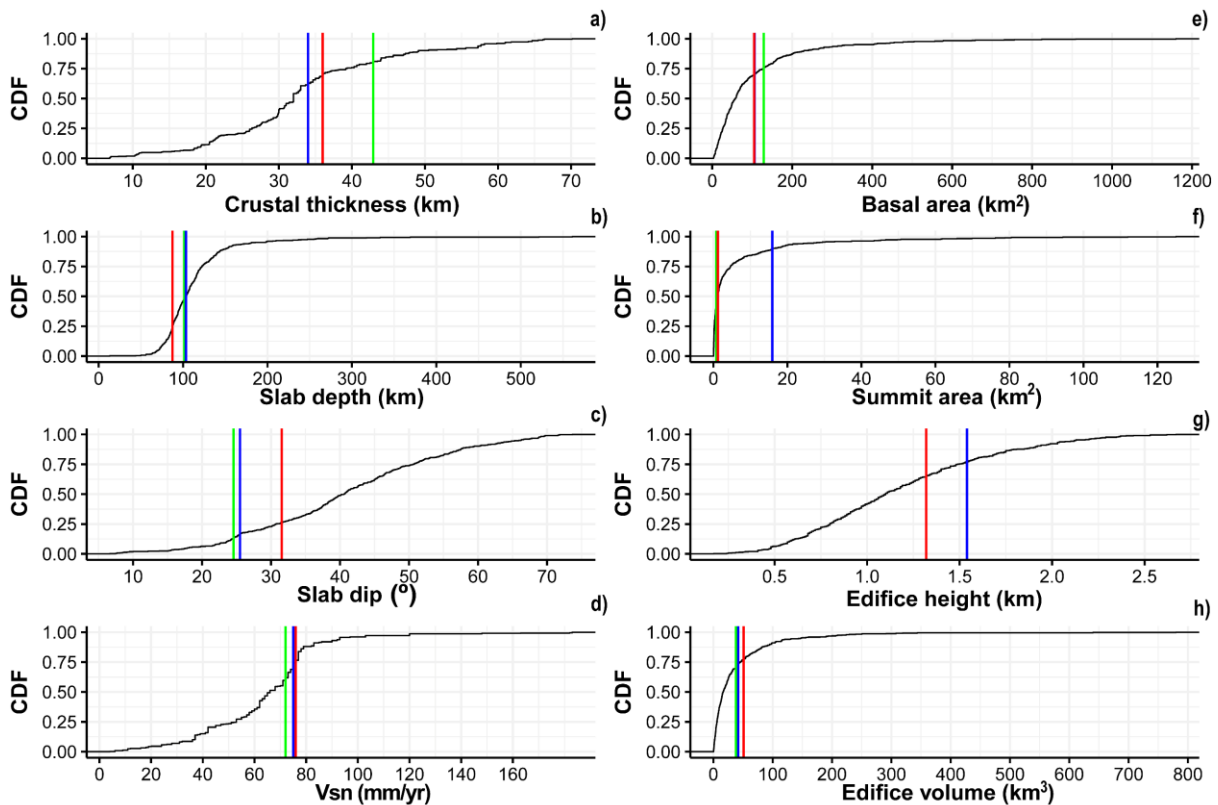
743 The dendrograms from the raw and weighted dataset (Fig. 2 and 6) indicate that the most similar  
744 volcano, and, therefore, best analogue, is Mocho-Choshuenco (Chile). Mocho-Choshuenco is a  
745 compound stratovolcano covered by glaciers, located 460 km from Melimoyu. The morphology of both  
746 volcanoes is very similar (Fig. 11e and 11h), except for the summit area and edifice height (Fig. 11h  
747 and 11g). The difference in the summit area can be explained by the fact that Grosse et al. (2013)  
748 calculated the morphology of the summit of Mocho-Choshuenco including both peaks. Like Melimoyu,  
749 Mocho-Choshuenco also has parasitic craters and basaltic scoria cones on the flanks, indicating  
750 monogenetic volcanism (Rawson et al., 2015). Both volcanoes have similar values for multiple  
751 parameters of the tectonic setting (e.g., crustal thickness, slab dip, slab depth, and normal component  
752 of the velocity of the subducting plate (Fig 11a-d)). We also see a strong similarity in the rock  
753 composition, with the rock types included in the GVP being identical in both volcanoes.

754 The VOTW database only reports two confirmed Holocene eruptions from Mocho-Choshuenco, the  
755 most recent in 1937 of unknown eruption size. The previous eruption, reported from historical  
756 observations in 1864, was classified as a VEI 2. Both eruptions were reported for Mocho stratovolcano.  
757 In addition, LaMEVE reports another three Holocene eruptions dated in  $1265 \text{ BP} \pm 110$ ,  $1580 \text{ BP} \pm 115$ ,  
758 and  $8202 \text{ BP} \pm 220$ , with a Magnitude of 4.6 (VEI 4), 5 (VEI 5), and 5.3 (VEI 5), respectively. Close to  
759 the Holocene boundary, there are two more Plinian eruptions dated in  $10189 \text{ BP} \pm 1361$  and  
760  $11391 \pm 1002$ , of Magnitude (M) 5.3 (VEI 5), and 5.7 (VEI 5), respectively. In addition to the data  
761 reported in the global databases, Rawson et al. (2015) report at least 34 post-glacial explosive eruptions,  
762 making Mocho-Choshuenco one of the most hazardous volcanoes from Chile in terms of the capacity  
763 to produce Plinian eruptions.

764 Using the reduced dataset as input, the dendrogram (Fig. 5) shows that the most similar volcano to  
765 Melimoyu is Tolhuaca (Chile). Tolhuaca is a snow-capped stratovolcano in the vicinity of Lonquimay,



766 also a potential analogue, 648 km from Melimoyu. We observe similar morphometric variables of  
 767 Tolhuaca and Melimoyu (Fig. 11 e-h). Regarding the tectonic setting variables, both volcanoes share  
 768 similar values of slab depth, slab dip, and normal component of the velocity of the subducting plate  
 769 (Fig. 11b-d). The composition from the GVP indicates that Tolhuaca produces mostly Andesite/Basaltic  
 770 Andesite and Basalt/Picro-Basalt, although there is evidence of Dacites (Polanco et al., 2000).  
 771 According to the VOTW database, Tolhuaca has four confirmed eruptions in the Holocene, the most  
 772 recent corresponding to the post-glacial (after 4000 BCE) basaltic activity (VEI 0) from the Pumehua  
 773 volcanic trend located in the NW flank of Tolhuaca (Naranjo (pers. comm. 2000) in Melosh et al.  
 774 (2012)). The remaining eruptions have been classified as VEI 3. There is no evidence of historical  
 775 eruptions, but there is currently fumarolic activity at the summit (Polanco et al., 2000; Sanchez-Alfaro  
 776 et al., 2016).



777

778 **Fig. 11.** Empirical CDF for a selection of tectonic setting parameters (a-d) and morphological  
 779 parameters (e-h) from the 438 subduction zone volcanoes included in the input dataset of the clustering.  
 780 The red, blue, and green lines indicate the value for Melimoyu, Mocho-Choshuenco, and Tolhuaca,  
 781 respectively. Note: x-axes are in different scales.

782 The selection of the 20 analogues for Melimoyu derived from the raw dataset was made by assessing  
 783 the similarity in the eruptive behaviour reflected in the dispersion of the absolute probability (Fig. 7)  
 784 and filtering the set of potential analogues with the set of criteria in section 4.3. The variability in the

785 results obtained from different input datasets shows the importance of combining expert knowledge  
786 with quantitative and objective approaches when assessing the suitability of analogue volcanoes.

787 From the 55 potential analogues in Figure 2, 14 volcanoes were excluded because they lack confirmed  
788 eruptions in the VOTW and LaMEVE database or only have eruptions without VEI, and we cannot use  
789 them to estimate an  $f$ - $M$  relationship. Therefore, 25% of the set of potential analogues are data-limited  
790 volcanoes. This could be seen as a limitation in our approach since we are not excluding volcanoes with  
791 scarce records from the clustering by not considering the eruptive history when defining analogues.  
792 However, we think this is an advantage of our approach since it allows for finding potential analogues  
793 for data-limited volcanoes and identifying where future geological studies could focus, assuming that  
794 these analogues have similar eruptive behaviour, and we are missing eruptions from these data-limited  
795 volcanoes. Furthermore, by not accounting for the eruptive behaviour in the input data, we can also  
796 identify analogues for potentially active volcanoes. This advantage is especially important for regions  
797 where eruptions from potentially active volcanoes are relatively frequent. This is the case for the  
798 volcanic region of South America, where nearly 40% of all the Holocene volcanoes are potentially  
799 active, and on average, a potentially active volcano has its First Recorded Eruption in the Holocene  
800 (FRESH) every eight years (Burgos et al., 2022a).

801 The criteria for filtering volcanoes into the analogue selection were defined with the goal of finding  
802 suitable analogues for estimating the empirical  $f$ - $M$  relationship. This approach led to excluding Llaima  
803 and Villarrica, two frequently active volcanoes with a history of large explosive eruptions ( $VEI \geq 4$ ) in  
804 the Holocene. Due to their current persistent activity and open-vent state (Ruth et al., 2016; Witter et  
805 al., 2004), they cannot be considered analogues of Melimoyu in terms of eruption recurrence, especially  
806 from small explosive eruptions in Villarrica (see outlier for  $VEI \leq 1$  and 2 eruptions from the raw dataset  
807 in Figure 7). However, the activity in Villarrica and Llaima has shifted between predominantly  
808 explosive to effusive and explosive episodes over time (Lara and Clavero, 2004; Lohmar et al., 2006,  
809 2005; Schindlbeck et al., 2014). These changes in eruption regimes suggest that Villarrica and Llaima  
810 might be in a different life stage than Melimoyu, meaning they could be analogues over longer  
811 timeframes covering regime changes with varying activity levels.

812 New methods for identifying analogues could integrate a temporal component to account for volcanic  
813 system life stages and cyclical changes, moving from a static to a dynamic analogue concept. Future  
814 work could explore the possibility of identifying ‘timeless’ and ‘contemporary’ analogues  
815 depending on whether the variables used remain constant or change within time windows shorter  
816 than the geological time scale (e.g., tectonic setting vs morphology).

817 Despite the differences in the current eruptive behaviour, the eruption history from volcanoes like  
818 Villarrica and Llaima can be useful for probabilistic modelling of volcanic hazards at Melimoyu,

819 providing data that inform the range of eruption characteristics that may be expected in the future. For  
820 example, eruption source parameters to model scenarios lacking in Melimoyu's records (e.g., effusive,  
821 or low explosive eruptions).

### 822 *6.3 Importance of the tectonic setting*

823 Ten out of 20 of the analogues, including Melimoyu, are in the SVZ (Fig.1a), suggesting that the  
824 characteristics of the tectonic setting strongly control the clustering. The influence that the Chile Triple  
825 Junction and the LOFZ have in the nature and distribution of volcanism in the SVZ (Cembrano and  
826 Lara, 2009; de Pascale et al., 2021; Gutiérrez et al., 2005; López Escobar et al., 1995; Stern et al., 2007),  
827 may explain why numerous volcanoes in this area share similar characteristics with Melimoyu.

828 Similarities in the tectonic setting are also observed among the volcanic arcs where the 20 analogues  
829 are located (Cascades, Northern Andes, Southern Andes, and Honshu). The range of some tectonic  
830 setting variables for our analogues, such as the age of the subducting plate (from 10 to 42 Ma) or the  
831 crustal thickness (from ~32 to 54 km), seems large. However, this range is relatively small compared  
832 to the global values from all the volcanic arcs (~5 to 156 Ma; ~6 to 73 km). The similarity in these  
833 values from analogues in distinct geographic settings shows that the clustering can identify patterns in  
834 the data describing the tectonic setting while making distinctions among volcanic arcs.

835 Numerous studies have discussed the role tectonics play in the volcanism of subduction zones (e.g.,  
836 Acocella (2014), Hughes and Mahood (2008, 2011), Sheldrake et al. (2020)). Heuret and Lallemand  
837 (2005) and Lallemand et al. (2005) discussed the relationship between the different components of  
838 subduction zones, some of which have also been found among the 438 volcanoes from our study (Fig.  
839 3) (e.g., age of the subducting plate and the slab thickness). The importance of the tectonic setting in  
840 the generation of different magma compositions (Hughes and Mahood, 2008, 2011; Sobradelo et al.,  
841 2010; Sheldrake et al., 2020) is also reflected in the weak correlation between the crustal thickness, slab  
842 dip, the normal component of the back arc strain-rate, and the presence of Basaltic and Dacitic magmas  
843 (Fig. 3). The age of the subducting plate, slab and crustal thickness, subducting velocity, and  
844 convergence obliquity were also highlighted by the PCA as variables contributing the most to  
845 explaining the variance in PC1 (Table 1). Some of these variables also had more importance (i.e., higher  
846 weights in supplementary material 4) when producing the minimum dispersion in the absolute  
847 probability from the analogues derived from the weighted dataset (Fig. 7).

848 The conditions of the tectonic setting are key to developing long-lived and large plumbing systems  
849 capable of generating large-magnitude explosive and caldera-forming eruptions (de Silva, 2008;  
850 Hughes and Mahood, 2011, 2008b; Weber and Sheldrake, 2022). According to Sheldrake et al. (2020),  
851 the crustal thickness, the age of the subducting plate, and the convergent obliquity influence the  
852 production of large-magnitude eruptions ( $4 \leq M \leq 7$ ). Their study establishes that volcanic arcs can be

853 classified into two groups with a distinct potential of having large magnitude eruptions based on the  
854 parameter  $H$  (i.e., a combination of the age of the slab and movement of the subduction plate). High- $H$   
855 regime volcanic arcs, characterised by low obliquity and moderate slab ages, are more likely to generate  
856 large-magnitude eruptions. The probability of producing large-magnitude eruptions in these volcanic  
857 arcs is strongly controlled by the convergent obliquity. In contrast, in low- $H$  regime, volcanic arcs with  
858 low mantle productivity and oblique convergence, the probability of generating large magnitude  
859 eruptions is lower and increases with the crustal thickness. Honshu arc, where Yakedake is located, is  
860 classified as High- $H$  regime by Sheldrake et al. (2020). In contrast, the Cascades, Northern Andes, and  
861 Southern Andes arcs, where 19 analogues are located, are classified by Sheldrake et al. (2020) as low-  
862  $H$  regimes and have notably similar slopes of the  $f$ - $M$  relationship ( $2.5 < \alpha < 3$  in their Figure 9d). These  
863 findings further support our decision to consider these volcanoes as analogues and explain why many  
864 potential analogues can produce large explosive eruptions.

#### 865 *6.4 Uncertainty in eruption probabilities*

866 Using eruption records from multiple analogues allows for defining the uncertainty around the  $f$ - $M$   
867 relationship estimations for Melimoyu. Relying on a small selection of analogues, as we do in this study,  
868 instead of global analogues defined from broad categories, has been proven effective for reducing the  
869 uncertainty in the probability estimations (Hayes et al., 2022). However, we must be cautious when  
870 interpreting the range of probabilities given by the  $f$ - $M$  relationship since, for some eruption sizes, the  
871 difference between the 5<sup>th</sup> and 95<sup>th</sup> percentile can be of several orders of magnitude (Table 3). This  
872 uncertainty can result from the variability in the eruption recurrence resulting from distinct eruptive  
873 behaviour or different degrees of data completeness among volcanoes, which is partially accounted for  
874 by using only eruption records since the RCD.

875 The discrepancies in the eruption data reported for Mocho-Choshuenco in the VOTW database, the  
876 LaMEVE database, and Rawson et al. (2015) show the importance of not relying only on global  
877 databases when assessing the volcanic hazard at individual volcanoes. While we used all available  
878 eruption data for Melimoyu and restricted our calculation of eruption probability to only the most  
879 complete portion of the VOTW database for all the analogues, we still recognise that the eruption  
880 probabilities presented in this study may have been under-estimated if eruption records are missing  
881 from any of the analogues. Differences among sources further support our decision to exclude the  
882 eruptive history from the VOTW database in the clustering input. Under-reporting in global databases  
883 can limit the ability of methods that define analogues based on eruption data from the VOTW database  
884 or LaMEVE (e.g., Tierz et al. (2019) and Wang et al. (2022)) to capture all or even the most appropriate  
885 analogues.

## 886 7. Conclusion

887 Identifying analogues for data-limited volcanoes is essential to reduce the uncertainty of volcanic  
888 hazard assessments. Analogues have been typically defined using categorical information and broad  
889 classes, which can lead to numerous analogues and large uncertainties in probability estimations. We  
890 have combined an objective and quantitative approach to identify groups of analogues that include  
891 Melimoyu, our volcano target of study, using agglomerative hierarchical clustering with an assessment  
892 of suitability based on the dispersion of probability estimates and expert knowledge.

893 This algorithm was applied to 37 variables describing the tectonic setting, rock composition, and  
894 morphology of 438 subduction zone volcanoes, including Melimoyu. A sensitivity analysis was  
895 performed using a raw, reduced, and weighted dataset to assess how the potential analogues change  
896 with the input data. We found that applying a PCA before the clustering (i.e., reduced dataset) generates  
897 a group of potential analogues with highly dispersed absolute probabilities. In contrast, the dispersion  
898 for the absolute probability estimated from the analogues derived from the raw and weighted dataset is  
899 lower. As expected, the dispersion is the lowest for the analogues from the weighted dataset since the  
900 weights were tuned to minimise the variability in the absolute probabilities across the set of analogues.

901 After applying the set of criteria deemed as important by SERNAGEOMIN and VB for estimating the  
902  $f$ - $M$  relationship for Melimoyu (i.e., available eruption data, history of large explosive eruptions, not  
903 frequently active, and a similar range of magma composition), we retain 20 analogues from the raw  
904 dataset, eight from the reduced dataset, and 13 from the weighted dataset. Considering the dispersion  
905 and the number of volcanoes that meet the criteria, we select the set of 20 volcanoes from the raw  
906 dataset as the best analogues for Melimoyu. The clustering of these volcanoes is strongly controlled by  
907 the characteristics of the tectonic setting at the volcanic arcs where they are located, which plays a key  
908 role in the  $f$ - $M$  relationships (Sheldrake et al., 2020). Furthermore, the influence of the Liquiñe-Ofqui  
909 Fault Zone on the volcanism of the Southern Volcanic Zone in Chile (Cembrano and Lara, 2009; de  
910 Pascale et al., 2021; Völker et al., 2011) explains why most of the analogues are from this area.

911 The  $f$ - $M$  relationship modelled from the analogue's eruption data reflects the low frequency of eruptions  
912 at Melimoyu and the history of highly explosive eruptions. For example, the probability of an eruption  
913 of any VEI is  $3.68 \times 10^{-3}$  (50<sup>th</sup> percentile) (i.e., average recurrence interval of ~272 years), which  
914 indicates long periods of recurrence between eruptions. Additionally, the conditional probability  
915 distribution indicates that in the event of an eruption at Melimoyu, there is a 49% probability that it will  
916 have a  $VEI \geq 4$  (50th percentile), reflecting the potential for large explosive eruptions at Melimoyu.  
917 Lastly, the product of the absolute and the conditional probability produces an annual probability of  
918  $4.8 \times 10^{-4}$ ,  $1.2 \times 10^{-3}$ ,  $1.5 \times 10^{-4}$ ,  $9.8 \times 10^{-4}$ , and  $8.3 \times 10^{-4}$  (50th percentile) for  $VEI \leq 1$ , 2, 3, 4, and  $VEI \geq 5$   
919 eruptions at Melimoyu, respectively.

920 The  $f$ - $M$  relationship presented in this study constitutes an important step towards preparing the official  
921 hazard map for Melimoyu. In addition, the probabilities and the analogues reported in this study will be  
922 used by SERNAGEOMIN to establish the recurrence of different eruptive scenarios that could be  
923 expected if Melimoyu reactivates. Future work will explore using the proposed analogues for Melimoyu  
924 to build a probabilistic event tree and define ESP for modelling volcanic hazards.

925 This study shows that using quantitative variables when defining analogues is essential to capture the  
926 diversity among volcanoes, helping to find smaller groups of volcanoes within broad categories and  
927 reducing the uncertainty in the  $f$ - $M$  relationship estimates. This approach can be combined with other  
928 proposed methods and expert knowledge to fine-tune the selection of analogues. Furthermore, the  
929 agglomerative hierarchical clustering can be easily applied to other volcanoes allowing the user to select  
930 multiple variables from the global database made available here.

## 931 **8. References**

932 Abdi, H., Williams, L.J., 2010. Principal component analysis. *Wiley Interdiscip Rev Comput Stat* 2,  
933 433–459. <https://doi.org/10.1002/wics.101>

934 Acocella, V., 2014. Structural control on magmatism along divergent and convergent plate  
935 boundaries: Overview, model, problems. *Earth Sci Rev* 136, 226–288.  
936 <https://doi.org/10.1016/j.earscirev.2014.05.006>

937 Acocella, V., di Lorenzo, R., Newhall, N., Scandone, R., 2015. An overview of recent (1988 to 2014)  
938 caldera unrest: Knowledge and perspectives. *Reviews of Geophysics* 53, 896–955.  
939 <https://doi.org/10.1029/88EO01108>

940 Acocella, V., Funicello, F., 2010. Kinematic setting and structural control of arc volcanism. *Earth*  
941 *Planet Sci Lett* 289, 43–53. <https://doi.org/10.1016/j.epsl.2009.10.027>

942 Aggarwal, C.C., Hinneburg, A., Keim, D.A., 2001. On the Surprising Behavior of Distance Metrics  
943 in High Dimensional Space, in: van den Bussche, J., Vianu, V. (Eds.), *Database Theory —*  
944 *ICDT 2001*. Springer Berlin Heidelberg, Berlin, Heidelberg, pp. 420–434.  
945 [https://doi.org/https://doi.org/10.1007/3-540-44503-X\\_27](https://doi.org/https://doi.org/10.1007/3-540-44503-X_27)

946 Assent, I., 2012. Clustering high dimensional data. *WIREs Data Mining Knowledge Discovery* 2,  
947 340–350. <https://doi.org/10.1002/widm.1062>

948 Banerjee, A., Davé, R.N., 2004. Validating clusters using the Hopkins statistic, in: *IEEE International*  
949 *Conference on Fuzzy Systems*. Budapest, pp. 149–153.  
950 <https://doi.org/10.1109/FUZZY.2004.1375706>

- 951 Bebbington, M.S., 2014. Long-term forecasting of volcanic explosivity. *Geophys J Int* 197, 1500–  
952 1515. <https://doi.org/10.1093/gji/ggu078>
- 953 Bebbington, M.S., Jenkins, S.F., 2022. Intra-Eruption Forecasting Using Analogue Volcano and  
954 Eruption Sets. *J Geophys Res Solid Earth* 127. <https://doi.org/10.1029/2022JB024343>
- 955 Bird, P., 2003. An updated digital model of plate boundaries. *Geochemistry, Geophysics,*  
956 *Geosystems* 4, 1027. <https://doi.org/10.1029/2001GC000252>
- 957 Boehmke, B., Greenwell, B., 2019. Hierarchical Clustering, in: *Hands-On Machine Learning with*  
958 *R*. Chapman and Hall/CRC, New York. <https://doi.org/10.1201/9780367816377>
- 959 Burgos, V., Jenkins, S.F., Bebbington, M., Newhall, C., Taisne, B., 2022a. What is the probability  
960 of unexpected eruptions from potentially active volcanoes or regions? *Bull Volcanol* 84, 84–  
961 97. <https://doi.org/10.1007/s00445-022-01605-0>
- 962 Burgos, V., Jenkins, S.F., Bebbington, M., Newhall, C., Taisne, B., 2022b. A new perspective on  
963 eruption data completeness: insights from the First Recorded EruptionS in the Holocene  
964 (FRESH) database. *Journal of Volcanology and Geothermal Research* 431, 107648.  
965 <https://doi.org/10.1016/j.jvolgeores.2022.107648>
- 966 Cembrano, J., Lara, L., 2009. The link between volcanism and tectonics in the southern volcanic  
967 zone of the Chilean Andes: A review. *Tectonophysics* 471, 96–113.  
968 <https://doi.org/10.1016/j.tecto.2009.02.038>
- 969 Chen, Peter.Y., Popovich, Paula.M., 2002. *Correlation : Parametric and Nonparametric Measures.*  
970 *Sage University Papers Series on Quantitative Applications in the Social Sciences* 07–139.
- 971 Crossweller, H.S., Arora, B., Brown, S.K., Cottrell, E., Deligne, N.I., Guerrero, N.O., Hobbs, L.,  
972 Kiyosugi, K., Loughlin, S.C., Lowndes, J., Nayembil, M., Siebert, L., Sparks, R.S.J.,  
973 Takarada, S., Venzke, E., 2012. Global database on large magnitude explosive volcanic  
974 eruptions (LaMEVE). *Journal of Applied Volcanology* 1, 1–13.  
975 <https://doi.org/10.1186/2191-5040-1-4>
- 976 Daros Idalino, F., Kellem da Rosa, K., Ferrando Acuña, F., Kozhikkodan Veetil, B., Cardia Simões,  
977 J., Souza, E., 2020. Recent glacier variations on Mount Melimoyu (44°50'S-72°51'W),  
978 Chilean Patagonia, using Sentinel-2 data. *Geocarto Int* 35, 1199–1213.  
979 <https://doi.org/10.1080/10106049.2018.1557262>
- 980 de Pascale, G.P., Froude, M., Penna, I., Hermanns, R.L., Sepúlveda, S.A., Moncada, D., Persico, M.,  
981 Easton, G., Villalobos, A., Gutiérrez, F., 2021. Lliquiñe-Ofqui's fast slipping intra-volcanic

- 982 arc crustal faulting above the subducted Chile Ridge. *Sci Rep* 11, 1–12.  
983 <https://doi.org/10.1038/s41598-021-86413-w>
- 984 de Silva, S., 2008. Arc magmatism, calderas, and supervolcanoes. *Geology* 36, 671–672.  
985 <https://doi.org/10.1130/focus082008.1>
- 986 Duque, A., González, K., Pérez, N., Benítez, D.S., 2020. Understanding the Cotopaxi Volcano  
987 Activity with Clustering-Based Approaches, in: Orjuela-Cañón, A.D., Lopez, J., Arias-  
988 Londoño, J.D., Figueroa-García, J.C. (Eds.), *IEEE Colombian Conference on Applications  
989 in Computational Intelligence, Communications in Computer and Information Science*.  
990 Springer International Publishing, Cham, pp. 3–15. [https://doi.org/10.1007/978-3-030-  
991 69774-7](https://doi.org/10.1007/978-3-030-69774-7)
- 992 Geoffroy, C., 2017. Eruptive parameters and pre-eruptive processes for late Holocene activity  
993 centred at Melimoyu Volcano, Southern Chile (44°05' S) (Master thesis ). Universidad de  
994 Chile, Santiago de Chile.
- 995 Geoffroy, C., Amigo, A., 2015. Avances en la Caracterización Tefrocronológica de la Actividad  
996 Explosiva Post-Glacial del Volcán Melimoyu, Chile, in: XIV Congreso Geológico Chileno.  
997 La Serena, pp. 194–197.
- 998 Geoffroy, C.A., Alloway, B. v., Amigo, À., Parada, M.A., Gutierrez, F., Castruccio, A., Pearce,  
999 N.J.G., Morgado, E., Moreno, P.I., 2018. A widespread compositionally bimodal tephra  
1000 sourced from Volcán Melimoyu (44° S, Northern Patagonian Andes): Insights into magmatic  
1001 reservoir processes and opportunities for regional correlation. *Quat Sci Rev* 100, 149–151.  
1002 <https://doi.org/https://doi.org/10.1016/j.quascirev.2018.09.034>
- 1003 Grosse, P., Euillades, P.A., Euillades, L.D., van Wyk de Vries, B., 2014. A global database of  
1004 composite volcano morphometry. *Bull Volcanol* 76, 1–16. [https://doi.org/10.1007/s00445-  
1005 013-0784-4](https://doi.org/10.1007/s00445-013-0784-4)
- 1006 Grosse, P., Kervyn, M., 2018. Morphometry of terrestrial shield volcanoes. *Geomorphology* 304, 1–  
1007 14. <https://doi.org/10.1016/j.geomorph.2017.12.017>
- 1008 Gutiérrez, F., Gioncada, A., González Ferran, O., Lahsen, A., Mazzuoli, R., 2005. The Hudson  
1009 Volcano and surrounding monogenetic centres (Chilean Patagonia): An example of  
1010 volcanism associated with ridge-Trench collision environment. *Journal of Volcanology and  
1011 Geothermal Research* 145, 207–233. <https://doi.org/10.1016/j.jvolgeores.2005.01.014>
- 1012 GVP, 2013. *Volcanoes of the World* (v. 4.8.5; 11 Feb 2020). Venzke E, editor. Smithsonian  
1013 Institution. <https://doi.org/doi.org/10.5479/si.GVP.VOTW4-2013>



- 1014 GVP, 2010. Report on Melimoyu (Chile). In: Sennert, S K (ed.), Weekly Volcanic Activity Report,  
1015 9 June-15 June 2010. [WWW Document]. Smithsonian Institution and US Geological  
1016 Survey.
- 1017 Han, J., Kamber, M., Pei, J., 2012. Data Preprocessing, in: Jiawei Han, Micheline Kamber, J.P. (Ed.),  
1018 Data Mining: Concepts and Techniques. Morgan kaufmann, pp. 83–124.  
1019 <https://doi.org/https://doi.org/10.1016/B978-0-12-381479-1.00003-4>.
- 1020 Hayes, G., 2018. Slab2: A Comprehensive Subduction Zone Geometry Model [WWW Document].  
1021 U.S. Geological Survey data release. URL  
1022 <https://www.sciencebase.gov/catalog/item/5aa1b00ee4b0b1c392e86467> (accessed 8.11.21).
- 1023 Hayes, G.P., Moore, G.L., Portner, D.E., Hearne, M., Flamme, H., Furtney, M., Smoczyk, G.M.,  
1024 2018. Slab2, a comprehensive subduction zone geometry model. *Science* (1979) 362, 58–  
1025 61. [https://doi.org/DOI: 10.1126/science.aat4723](https://doi.org/DOI:10.1126/science.aat4723)
- 1026 Hayes, J.L., Jenkins, S.F., Joffrain, M., 2022. Large Uncertainties Are Pervasive in Relationships for  
1027 Volcanoes in Southeast Asia. *Frontier in Earth Science* 10, 1–19.  
1028 <https://doi.org/10.3389/feart.2022.895756>
- 1029 Herman, F., Brandon, M., 2015. Mid-latitude glacial erosion hotspot related to equatorial shifts in  
1030 southern Westerlies. *Geology* 43, 987–990. <https://doi.org/10.1130/G37008.1>
- 1031 Heuret, A., 2006. Dynamique des zones de subduction: étude statistique globale et approche  
1032 analogique. Université Montpellier II.
- 1033 Heuret, A., Lallemand, S., 2005. Plate motions, slab dynamics and back-arc deformation. *Physics of*  
1034 *the Earth and Planetary Interiors* 149, 31–51. <https://doi.org/10.1016/j.pepi.2004.08.022>
- 1035 Hone, D.W.E., Mahony, S.H., Sparks, R.S.J., Martin, K.T., 2007. Cladistic analysis applied to the  
1036 classification of volcanoes. *Bull Volcanol* 70, 203–220. [https://doi.org/10.1007/s00445-007-](https://doi.org/10.1007/s00445-007-0132-7)  
1037 [0132-7](https://doi.org/10.1007/s00445-007-0132-7)
- 1038 Hughes, G.R., Mahood, G.A., 2011. Silicic calderas in arc settings: Characteristics, distribution, and  
1039 tectonic controls. *Bulletin of the Geological Society of America* 123, 1577–1595.  
1040 <https://doi.org/10.1130/B30232.1>
- 1041 Hughes, G.R., Mahood, G.A., 2008a. Tectonic controls on the nature of large silicic calderas in  
1042 volcanic arcs. *Geology* 36, 627–630. <https://doi.org/10.1130/G24796A.1>
- 1043 Hughes, G.R., Mahood, G.A., 2008b. Tectonic controls on the nature of large silicic calderas in  
1044 volcanic arcs. *Geology* 36, 627–630. <https://doi.org/10.1130/G24796A.1>
- 1045 Instituto Nacional de Estadísticas, 2019. Síntesis de Resultados Censo 2017, Región de Ayesén.

- 1046 Jenkins, S., Magill, C., McAneney, J., Blong, R., 2012a. Regional ash fall hazard I: A probabilistic  
1047 assessment methodology. *Bull Volcanol* 74, 1699–1712. [https://doi.org/10.1007/s00445-](https://doi.org/10.1007/s00445-012-0627-8)  
1048 012-0627-8
- 1049 Jenkins, S., McAneney, J., Magill, C., Blong, R., 2012b. Regional ash fall hazard II: Asia-Pacific  
1050 modelling results and implications. *Bull Volcanol* 74, 1713–1727.  
1051 <https://doi.org/10.1007/s00445-012-0628-7>
- 1052 Jenkins, S.F., Biass, S., Williams, G.T., Hayes, J.L., Tennant, E., Yang, Q., Burgos, V., Meredith,  
1053 E.S., Lerner, G.A., Syarifuddin, M., Verolino, A., 2022. Evaluating and ranking Southeast  
1054 Asia’s exposure to explosive volcanic hazards. *Natural Hazards and Earth System Sciences*  
1055 22, 1233–1265. <https://doi.org/10.5194/nhess-22-1233-2022>
- 1056 Jolliffe, I.T., Cadima, J., 2016. Principal component analysis: A review and recent developments.  
1057 *Philosophical Transactions of the Royal Society A: Mathematical, Physical and Engineering*  
1058 *Sciences* 374. <https://doi.org/10.1098/rsta.2015.0202>
- 1059 Kaufman, L., Rousseeuw, P.J., 1991. Chapter 5: Agglomerative Nesting (Program AGNES), in:  
1060 Finding Groups in Data: An Introduction to Cluster Analysis. John Wiley & Sons, Inc.,  
1061 Hoboken, New Jersey, pp. 199–252.
- 1062 Lallemand, S., Heuret, A., Boutelier, D., 2005. On the relationships between slab dip, back-arc stress,  
1063 upper plate absolute motion, and crustal nature in subduction zones. *Geochemistry,*  
1064 *Geophysics, Geosystems* 6. <https://doi.org/10.1029/2005GC000917>
- 1065 Lara, L.E., Clavero, J., 2004. Villarrica Volcano (39.5 S), Southern Andes, Chile, Jorge Clavero.  
1066 Servicio Nacional de Geología y Minería.
- 1067 Laske, G., Masters, G., Ma, Z., Pasyanos, M., 2013. Update on CRUST1.0: A 1-degree global model  
1068 of Earth’s crust, in: EGU General Assembly 2013. p. 2658.
- 1069 Lawson, R.G., Jurs, P.C., 1990. New index for clustering tendency and its application to chemical  
1070 problems. *Journal of chemical information and computer science* 30, 36–41.  
1071 <https://doi.org/https://doi.org/10.1021/ci00065a010>
- 1072 Lindsay, J.M., Robertson, R.E.A., 2018. Integrating volcanic hazard data in a systematic approach  
1073 to develop volcanic hazard maps in the lesser antilles. *Front Earth Sci (Lausanne)* 6.  
1074 <https://doi.org/10.3389/feart.2018.00042>
- 1075 Lohmar, S., Parada, M.Á., Robin, C., Gerbe, M.C., Deniel, C., Gourgaud, A., López-Escobar, L.,  
1076 Moreno, H., Naranjo, J.A., 2006. Origin of postglacial “Mafic” ignimbrites at Llaima and

- 1077 Villarrica volcanoes (Southern Andes, Chile): Assimilation of plutonic rocks as one of the  
1078 triggering factors? *Simposio Sudamericano de Geología Isotópica (SSAGI) 5*, 417–421.
- 1079 Lohmar, S., Robin, C., Parada, M.A., Gourgaud, A., Lopez-Escobar, L., Moreno, H., Naranjo, J.,  
1080 2005. The two major postglacial (13-14,000 BP) pyroclastic eruptions of Llaima and  
1081 Villarrica volcanoes (Southern Andes): A comparison, in: *6th International Symposium on  
1082 Andean Geodynamics*. Barcelona, pp. 442–445.
- 1083 López Escobar, Á., Cembrano, J., Moreno, H., 1995. Geochemistry and tectonics of the Chilean  
1084 Southern Andes basaltic Quaternary volcanism (37-46°S). *Andean Geology* 22, 219–234.  
1085 <https://doi.org/10.5027/andgeoV22n2-a06>
- 1086 Loughlin, Sparks, R.S.J., Brown, S.K., Jenkins, S. F., Vye-Brown, C., 2015. Global volcanic hazards  
1087 and risk, *Global Volcanic Hazards and Risk*. Cambridge University Press.  
1088 <https://doi.org/10.1017/CBO9781316276273>
- 1089 Marín, A., 2014. Palena, Quitalco y Melimoyu: Intentos fallidos de colonización en el litoral de la  
1090 Región de Aysén (1889-1983). *Revista Austral de Ciencias Sociales* 137–156.  
1091 <https://doi.org/10.4206/rev.austral.cienc.soc.2014.n27-06>
- 1092 Marzocchi, W., Sandri, L., Gasparini, P., Newhall, C., Boschi, E., 2004. Quantifying probabilities of  
1093 volcanic events: The example of volcanic hazard at Mount Vesuvius. *J Geophys Res Solid  
1094 Earth* 109, 1–18. <https://doi.org/10.1029/2004JB003155>
- 1095 Mastin, L.G., Guffanti, M., Servranckx, R., Webley, P., Barsotti, S., Dean, K., Durant, A., Ewert,  
1096 J.W., Neri, A., Rose, W.I., Schneider, D., Siebert, L., Stunder, B., Swanson, G., Tupper, A.,  
1097 Volentik, A., Waythomas, C.F., 2009. A multidisciplinary effort to assign realistic source  
1098 parameters to models of volcanic ash-cloud transport and dispersion during eruptions.  
1099 *Journal of Volcanology and Geothermal Research* 186, 10–21.  
1100 <https://doi.org/10.1016/j.jvolgeores.2009.01.008>
- 1101 McInnes, L., Healy, J., Melville, J., 2020. UMAP: Uniform Manifold Approximation and Projection  
1102 for Dimension Reduction. *arXiv preprint arXiv:1802.03426*.
- 1103 Mead, S., Magill, C., 2014. Determining change points in data completeness for the Holocene  
1104 eruption record. *Bull Volcanol* 76. <https://doi.org/10.1007/s00445-014-0874-y>
- 1105 Melnick, D., Maldonado, V., Contreras, M., 2020. Database of active and potentially-active  
1106 continental faults in Chile at 1:25,000 scale. PANGAEA.

- 1107 Melosh, G., Moore, J., Stacey, R., 2012. Natural Reservoir Evolution in The Tolhuaca Geothermal  
1108 Field, Southern Chile. PROCEEDINGS, Thirty-Sixth Workshop on Geothermal Reservoir  
1109 Engineering.
- 1110 Mohamad, I. Bin, Usman, D., 2013. Standardization and its effects on K-means clustering algorithm.  
1111 Research Journal of Applied Sciences, Engineering and Technology 6, 3299–3303.  
1112 <https://doi.org/10.19026/rjaset.6.3638>
- 1113 Naranjo, J.A., Stern, C.R., 2004. Holocene tephrochronology of the southernmost part (42°30'–45°S)  
1114 of the Andean Southern Volcanic Zone. Revista Geologica de Chile 31, 225–240.  
1115 <https://doi.org/10.4067/S0716-02082004000200003>
- 1116 Newhall, C.G., 1982. A method for estimating intermediate and long-term risks from volcanic  
1117 activity, with an example from Mount St. Helens, Washington (No. 82-396). US Geological  
1118 Survey.
- 1119 Newhall, C.G., Costa, F., Ratdomopurbo, A., Venezky, D.Y., Widiwijayanti, C., Win, N.T.Z., Tan,  
1120 K., Fajiculay, E., 2017. WOVOdat – An online, growing library of worldwide volcanic  
1121 unrest. Journal of Volcanology and Geothermal Research 345, 184–199.  
1122 <https://doi.org/10.1016/j.jvolgeores.2017.08.003>
- 1123 Newhall, C.G., Pallister, J.S., 2015. Using Multiple Data Sets to Populate Probabilistic Volcanic  
1124 Event Trees, Volcanic Hazards, Risks, and Disasters. Elsevier Inc.  
1125 <https://doi.org/10.1016/B978-0-12-396453-3.00008-3>
- 1126 Paguican, E.M., Grosse, P., Fabbro, G.N., Kervyn, M., 2021. Morphometric classification and spatial  
1127 distribution of Philippine volcanoes. Journal of Volcanology and Geothermal Research 418,  
1128 107251. <https://doi.org/10.1016/j.jvolgeores.2021.107251>
- 1129 Polanco, E., Naranjo, J., Young, S., Moreno, H., 2000. Volcanismo Explosivo Holoceno en la  
1130 Cuenca del Alto Biobio, Andes del Sur (37°45'–38°30'S), in: IX Congreso Geológico  
1131 Chileno: Puerto Varas, 31 de Julio al 4 de Agosto, 2000.
- 1132 Rawson, H., Naranjo, J.A., Smith, V.C., Fontijn, K., Pyle, D.M., Mather, T.A., Moreno, H., 2015.  
1133 The frequency and magnitude of post-glacial explosive eruptions at Volcán Mocho-  
1134 Choshuenco, southern Chile. Journal of Volcanology and Geothermal Research 299, 103–  
1135 129. <https://doi.org/10.1016/j.jvolgeores.2015.04.003>
- 1136 Rodado, A., Bebbington, M., Noble, A., Cronin, S., Jolly, G., 2011. On Selection of Analog  
1137 Volcanoes. Math Geosci 43, 505–519. <https://doi.org/10.1007/s11004-011-9345-6>

- 1138 Rojas Hoppe, C., Subiabre, A., 1998. La Carretera Austral Entre Puerto Montt y La Junta (Región  
1139 Sur de Chile) y Sus Amenazas Naturales. Cuadernos de Geografía: Revista Colombiana de  
1140 Geografía 7, 50–69.
- 1141 Runge, M.G., Bebbington, M.S., Cronin, S.J., Lindsay, J.M., Kenedi, C.L., Moufti, M.R.H., 2014.  
1142 Vents to events: Determining an eruption event record from volcanic vent structures for the  
1143 Harrat Rahat, Saudi Arabia. *Bull Volcanol* 76, 1–16. <https://doi.org/10.1007/s00445-014-0804-z>  
1144
- 1145 Sanchez-Alfaro, P., Reich, M., Arancibia, G., Pérez-Flores, P., Cembrano, J., Driesner, T., Lizama,  
1146 M., Rowland, J., Morata, D., Heinrich, C.A., Tardani, D., Campos, E., 2016. Physical,  
1147 chemical and mineralogical evolution of the Tolhuaca geothermal system, southern Andes,  
1148 Chile: Insights into the interplay between hydrothermal alteration and brittle deformation.  
1149 *Journal of Volcanology and Geothermal Research* 324, 88–104.  
1150 <https://doi.org/10.1016/j.jvolgeores.2016.05.009>
- 1151 Sandri, L., Jolly, G., Lindsay, J., Howe, T., Marzocchi, W., 2012. Combining long- and short-term  
1152 probabilistic volcanic hazard assessment with cost-benefit analysis to support decision  
1153 making in a volcanic crisis from the Auckland Volcanic Field, New Zealand. *Bull Volcanol*  
1154 74, 705–723. <https://doi.org/10.1007/s00445-011-0556-y>
- 1155 Sandri, L., Thouret, J.C., Constantinescu, R., Biass, S., Tonini, R., 2014. Long-term multi-hazard  
1156 assessment for El Misti volcano (Peru). *Bull Volcanol* 76, 1–26.  
1157 <https://doi.org/10.1007/s00445-013-0771-9>
- 1158 Schindlbeck, J.C., Freundt, A., Kutterolf, S., 2014. Major changes in the post-glacial evolution of  
1159 magmatic compositions and pre-eruptive conditions of Llaima Volcano, Andean Southern  
1160 Volcanic Zone, Chile. *Bull Volcanol* 76, 1–22. <https://doi.org/10.1007/s00445-014-0830-x>
- 1161 SERNAGEOMIN, 2019. Ranking de Riesgo Específico de Volcanes Activos de Chile 2019.
- 1162 Sheldrake, T., 2014. Long-term forecasting of eruption hazards: A hierarchical approach to merge  
1163 analogous eruptive histories. *Journal of Volcanology and Geothermal Research* 286, 15–23.  
1164 <https://doi.org/10.1016/j.jvolgeores.2014.08.021>
- 1165 Sheldrake, T., Caricchi, L., 2017. Regional variability in the frequency and magnitude of large  
1166 explosive volcanic eruptions. *Geology* 45, 111–114. <https://doi.org/10.1130/G38372.1>
- 1167 Sheldrake, T.E., Scutari, M., Caricchi, L., 2020. Tectonic controls on global variations in the record  
1168 of large-magnitude explosive eruptions in volcanic arcs. *Front Earth Sci (Lausanne)* 8, 1–14.  
1169 <https://doi.org/10.3389/feart.2020.00127>

- 1170 Siebert, L., Cottrell, E., Venzke, E., Edwards, B., 2015. Catalog of Earth's Documented Holocene  
1171 Eruptions, Second Edi. ed, The Encyclopedia of Volcanoes. Elsevier Inc.  
1172 <https://doi.org/10.1016/b978-0-12-385938-9.15002-3>
- 1173 Siebert, L., Simkin, T., Kimberly, P., 2011. Volcanoes of the World. Univ of California Press.
- 1174 Sobradelo, R., Geyer, A., Martí, J., 2010. Statistical data analysis of the CCDB (Collapse Caldera  
1175 Database): Insights on the formation of caldera systems. Journal of Volcanology and  
1176 Geothermal Research 198, 241–252. <https://doi.org/10.1016/j.jvolgeores.2010.09.003>
- 1177 Solow, A.R., 2001. An Empirical Bayes Analysis of Volcanic Eruptions. Math Geol 33, 95–102.  
1178 <https://doi.org/10.1023/A:1007514410745>
- 1179 Stern, C.R., De Porras, M.E., Maldonado, A., 2015. Tefrocronología en curso superior del valle del  
1180 río Cisne (44°S), Chile Austral. Andean Geology 42, 173–189.  
1181 <https://doi.org/10.5027/andgeoV42n2-a02>
- 1182 Stern, C.R., Moreno, H., López-Escobar, L., Clavero, J.E., Lara, L.E., Naranjo, J.A., Parada, M.A.,  
1183 Skewes, M.A., 2007. Chilean volcanoes, in: Moreno, T., Gibbons, W. (Eds.), The Geology  
1184 of Chile. Geological Society of London. <https://doi.org/https://doi.org/10.1144/GOCH.5>
- 1185 Strauss, T., Von Maltitz, M.J., 2017. Generalising ward's method for use with manhattan distances.  
1186 PLoS One 12, 1–21. <https://doi.org/10.1371/journal.pone.0168288>
- 1187 Szakács, A., 1994. Redefining active volcanoes: a discussion. Bull Volcanol 56, 321–325.  
1188 <https://doi.org/10.1007/BF00326458>
- 1189 Tennant, E., Jenkins, S.F., Winson, A., Widiwijayanti, C., Gunawan, H., Haerani, N., Kartadinata,  
1190 N., Banggur, W., Triastuti, H., 2021. Reconstructing eruptions at a data limited volcano: A  
1191 case study at Gede (West Java). Journal of Volcanology and Geothermal Research 418.  
1192 <https://doi.org/10.1016/j.jvolgeores.2021.107325>
- 1193 Tierz, P., Clarke, B., Calder, E.S., Dessalegn, F., Lewi, E., Yirgu, G., Fontijn, K., Crummy, J.M.,  
1194 Bekele, Y., Loughlin, S.C., 2020. Event Trees and Epistemic Uncertainty in Long-Term  
1195 Volcanic Hazard Assessment of Rift Volcanoes: The Example of Aluto (Central Ethiopia).  
1196 Geochemistry, Geophysics, Geosystems 21. <https://doi.org/10.1029/2020GC009219>
- 1197 Tierz, P., Loughlin, S.C., Calder, E.S., 2019. VOLCANS: an objective, structured and reproducible  
1198 method for identifying sets of analogue volcanoes. Bull Volcanol 81.  
1199 <https://doi.org/10.1007/s00445-019-1336-3>
- 1200 Unglert, K., Radić, V., Jellinek, A.M., 2016. Principal component analysis vs. self-organizing maps  
1201 combined with hierarchical clustering for pattern recognition in volcano seismic spectra.

- 1202 Journal of Volcanology and Geothermal Research 320, 58–74.  
1203 <https://doi.org/10.1016/j.jvolgeores.2016.04.014>
- 1204 Völker, D., Kutterolf, S., Wehrmann, H., 2011. Comparative mass balance of volcanic edifices at the  
1205 southern volcanic zone of the Andes between 33°S and 46°S. *Journal of Volcanology and*  
1206 *Geothermal Research* 205, 114–129. <https://doi.org/10.1016/j.jvolgeores.2011.03.011>
- 1207 Wang, T., Bebbington, M., Cronin, S., Carman, J., 2022. Forecasting Eruptions at Poorly Known  
1208 Volcanoes Using Analogs and Multivariate Renewal Processes. *Geophys Res Lett* 49, 1–14.  
1209 <https://doi.org/10.1029/2021gl096715>
- 1210 Watt, S.F.L., Pyle, D.M., Mather, T.A., 2009. The influence of great earthquakes on volcanic  
1211 eruption rate along the Chilean subduction zone. *Earth Planet Sci Lett* 277, 399–407.  
1212 <https://doi.org/10.1016/j.epsl.2008.11.005>
- 1213 Weber, G., Sheldrake, T.E., 2022. Geochemical variability as an indicator for large magnitude  
1214 eruptions in volcanic arcs. *Sci Rep* 12, 15854. <https://doi.org/10.1038/s41598-022-19902-1>
- 1215 Weller, D.J., de Porras, M.E., Maldonado, A., Méndez, C., Stern, C.R., 2017. Tefrocronología  
1216 holocena del curso inferior del valle de río Cisnes, Chile austral. *Andean Geology* 44, 229–  
1217 248. <https://doi.org/10.5027/andgeov44n3-a01>
- 1218 Whelley, P.L., Newhall, C.G., Bradley, K.E., 2015. The frequency of explosive volcanic eruptions  
1219 in Southeast Asia. *Bull Volcanol* 77. <https://doi.org/10.1007/s00445-014-0893-8>
- 1220 Wils, K., van Daele, M., Lastras, G., Kissel, C., Lamy, F., Siani, G., 2018. Holocene Event Record  
1221 of Aysén Fjord (Chilean Patagonia): An Interplay of Volcanic Eruptions and Crustal and  
1222 Megathrust Earthquakes. *J Geophys Res Solid Earth* 123, 324–343.  
1223 <https://doi.org/10.1002/2017JB014573>
- 1224 Xu, D., Tian, Y., 2015. A Comprehensive Survey of Clustering Algorithms. *Annals of Data Science*  
1225 2, 165–193. <https://doi.org/10.1007/s40745-015-0040-1>

1226

## 1227 **9. Data Availability**

1228 The datasets generated in this study are included in the supplementary material and deposited in the  
1229 NTU open access research data repository DR-NTU (Data).

1230 Supplementary material 1: [https://researchdata.ntu.edu.sg/privateurl.xhtml?token=b64c61fd-92f3-](https://researchdata.ntu.edu.sg/privateurl.xhtml?token=b64c61fd-92f3-4ed5-a44f-db6d9c3822e3)  
1231 [4ed5-a44f-db6d9c3822e3](https://researchdata.ntu.edu.sg/privateurl.xhtml?token=b64c61fd-92f3-4ed5-a44f-db6d9c3822e3)

1232 Supplementary material 2: <https://researchdata.ntu.edu.sg/privateurl.xhtml?token=524101a7-649e-4b3f-9058-38aaaadaf283>

1234 Supplementary material 3: <https://researchdata.ntu.edu.sg/privateurl.xhtml?token=fca48c8b-78a1-4e9f-a98a-53484096a530>

1236 Supplementary material 4: <https://researchdata.ntu.edu.sg/privateurl.xhtml?token=330db840-c9f8-4354-b4f5-8f4d46a862cc>

1238 Supplementary material 5: <https://researchdata.ntu.edu.sg/privateurl.xhtml?token=f4e2848d-c0b2-42ab-aff8-368359b24a2e>

## 1240 **10. Author contributions**

1241 VB, SJ, LBT, CPM, MB, CN, AA, and BT contributed to the project idea, goals, and objectives.  
1242 VB developed the methodology with input from SJ, LBT, CPM, MB, JPA, and BT. VB  
1243 processed the data, analysed the results, prepared the figures, and wrote the manuscript. All  
1244 authors read, reviewed, and approved the final version of the manuscript.

## 1245 **11. Acknowledgements**

1246 We would like to thank Pablo Tierz, Tom Sheldrake, Elly Tennant, and Christina Widiwijayanti for the  
1247 fruitful discussions about volcanic analogues. We are also grateful to Constanza Jorquera Flores for the  
1248 numerous meetings about Melimoyu.

## 1249 **12. Funding**

1250 This research was supported by the Earth Observatory of Singapore via its funding from the National  
1251 Research Foundation Singapore and the Singapore Ministry of Education under the Research Centres  
1252 of Excellence initiative. This work comprises EOS contribution number 504. MB was supported by the  
1253 Resilience to Nature's Challenges Volcano program, New Zealand (contract number GNS-RNC047).

1254